



Photoemission and optical investigation of the electronic structure of molybdenum and ruthenium
by Kenneth Albert Kress

A thesis submitted to the Graduate Faculty in partial fulfillment of the requirements for the degree of
DOCTOR OF PHILOSOPHY in Physics

Montana State University

© Copyright by Kenneth Albert Kress (1969)

Abstract:

The photoemission and optical properties of vapor deposited films of molybdenum (Mo) and ruthenium (Ru) have been measured at room temperature. The photoemission properties measured are in the spectral range of the threshold (4.3 eV and 5.4 eV for Mo and Ru respectively) to 11.8 eV.

The optical properties are measured from 0.5 to 11.8 eV. The data from both Mo and Ru are found to be consistent with, and analyzed by, the nondirect transition model. Corrections for the escaping scattered electrons are included in the optical density of states (ODS) analysis. Peaks in the ODS are found at $E - E_F = -0.5$ eV, -1.6 eV, and -3.9 eV for Mo; and -0.4 eV, -1.3 eV, and a third tentatively placed at -3.6 eV for Ru.

The ODS for $E > E_p$ is determined by direct numerical inversion of the nondirect model expression for the dielectric constant. Several peaks appear in the ODS of Mo for $E > E_F$ while only one is observed in the ODS of Ru. The ODS of Mo and Ru is compared with the band calculations of Matthesis for tungsten (Matthesis, 1965) and rhenium (Matthesis, 1966) respectively. The relation of the measured ODS's to the explanations based on the electronic density of states for the anomalous isotopic mass dependence of the superconducting transition temperature is discussed. For Mo the volume loss function has a peak at 10.8 eV while the absorption coefficient has a minimum at 11.3 eV, which correlates with a minimum in the quantum yield at approximately 11.0 eV. The energy distribution of the photo-emitted electrons show slight structural changes in the spectral range, 10 to 11 eV. In the same spectral region a similar but weaker correlation between structure in the loss function, absorption coefficient, yield, and the energy distributions of Ru is noted.

PHOTOEMISSION AND OPTICAL INVESTIGATION OF THE ELECTRONIC
STRUCTURE OF MOLYBDENUM AND RUTHENIUM

by

KENNETH ALBERT KRESS

A thesis submitted to the Graduate Faculty in partial
fulfillment of the requirements for the degree

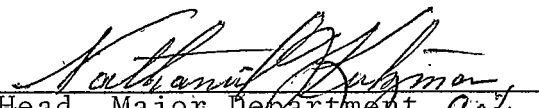
of

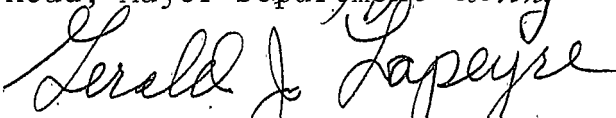
DOCTOR OF PHILOSOPHY

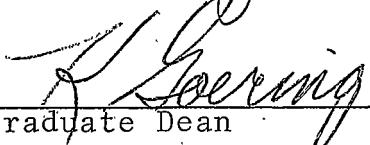
in

Physics

Approved:


Head, Major Department Acting


Chairman, Examining Committee


Graduate Dean

MONTANA STATE UNIVERSITY
Bozeman, Montana

December 1969

ACKNOWLEDGMENT

The author wishes to extend sincere thanks to Dr. Gerald J. Lapeyre, his thesis advisor, for guidance and constructive criticism made throughout the course of this work. His aid was especially helpful during the preparation of this manuscript. Discussions with Dr. A. J. M. Johnson, Dr. M. Rugheimer, Dr. N. Moise, Dr. K. Nordtvedt, and Mr. G. Stensland also proved valuable. The contributions of Mr. C. Badgley and Mr. F. Blankenburg in the mechanical design, electrical design, and the construction of part of the apparatus used in this investigation was certainly appreciated. The financial support of the National Aeronautics and Space Administration, the Air Force Office of Scientific Research, and Montana State University are gratefully acknowledged. Special thanks should be extended to my wife for the drafting of the various figures and the typing of the manuscript.

TABLE OF CONTENTS

Chapter		Page
I	INTRODUCTION	1
II	PHOTOEMISSION AND OPTICAL PROPERTIES OF METALS	5
	A. Optical Constants	7
	B. Photoemission	11
	1. Photoexcitation	12
	2. Transport and Escape	16
	3. Photoemitted Electrons	17
	4. Quantum Yield	19
	5. Scattered Electrons in the Energy Distribution Curves	19
	C. Optical Density of States Analysis	23
	D. Summary	32
III	EXPERIMENTAL PROCEDURES AND EQUIPMENT	34
	A. Photoemission Measurements	34
	1. Basic Experimental Apparatus and Procedures	34
	2. Vacuum Equipment and Procedures	37
	3. Sample Preparation	39
	4. Energy Distribution Curve Measurement	39
	5. Quantum Yield	41
	B. Optical Measurements	44
	1. Reflectometer	46
	C. Data Reproducibility	49
IV	MOLYBDENUM EXPERIMENTAL RESULTS	53
	A. Optical Measurements	53
	1. Reflectance	53
	2. Dielectric Constant	60
	3. Loss Functions	61
	4. Alpha, $(h\nu)n(h\nu)$, $(h\nu)^2 \epsilon_2(h\nu)$	63
	5. Sum Rules	65
	B. Photoemission Measurements	65
	1. Yield	66
	2. Energy Distribution Curves	68
	3. Optical Density of States for Molybdenum	71
	C. Summary	80

Table of Contents Continued

Chapter		Page
V	RUTHENIUM EXPERIMENTAL RESULTS	82
	A. Optical Measurements	82
	1. Reflectance	82
	2. Dielectric Constant	85
	3. Loss Functions	86
	4. Alpha, $(h\nu)n(h\nu)$, $(h\nu)^2 \epsilon_2(h\nu)$	86
	5. Sum Rules	86
	B. Photoemission Measurements	89
	1. Quantum Yield	90
	2. Energy Distribution Curves	92
	3. Optical Density of States for Ruthenium	95
	C. Summary	102
VI	INTERPRETATION AND CONCLUSIONS	104
	A. Optical Density of States and Band Structure of Molybdenum and Ruthenium	104
	1. Molybdenum	104
	2. Ruthenium	114
	3. Nondirect and Direct Transitions in Molybdenum and Ruthenium	118
	B. The Optical Density of States and Isotropic Mass Effect in Molybdenum and Ruthenium	120
	APPENDIX A: Kramers-Kronig Analysis	126
	APPENDIX B: Study of Cesium Covered Ruthenium	132
	LITERATURE CITED	138

LIST OF TABLES

Table		Page
I	Comparison of Optical Constants of Molybdenum of Present Study with those Measured by Others	59
II	Rigid Band Model Applied to the Theoretical Calculation of the Density of States of Cr and W	108
III	Rigid Band Model Applied to the Experimental Observation of the Density of States of Cr and Mo	110

LIST OF FIGURES

Figure		Page
1	Hypothetical Density of States for a Transition Metal. Shaded Area Represents Occupied or Initial States and Open Area Represents Unoccupied or Final States	13
2	Free Electron Threshold Function in Units of the Photoelectric Work Function, ϕ	18
3	Electron-Electron Scattering Event	21
4	Hypothetical EDC Structure Plot	27
5	Schematic of Basic Apparatus Used in Photoemission Experiment	35
6	Schematic of Vacuum Chamber for Photoemission Studies	38
7	Quantum Yield of Gold Compared to that taken by Krolikowski	45
8	Schematic of Reflectometer used for Reflectance Measurements	47
9	Direct Tracing of Experimental Energy Distribution Curves for $h\nu = 10.2$ eV from Experimental Chart	50
10	Summary of Reflectance Measurements for Molybdenum	54
11	Reflectance of Molybdenum where i is the Angle of Incidence	58
12	Dielectric Function of Molybdenum	58
13	Loss Functions for Molybdenum	62
14	Absorption Coefficient α for Molybdenum	62
15	Optical Functions $(h\nu)n(h\nu)$ and $(h\nu)^2 \epsilon_2(h\nu)$ for Molybdenum	64

List of Figures Continued

Figure		Page
16	Interband N_{IB} , Surface Plasma N_{SP} , and Volume Plasma N_{VP} Sum Rules for Molybdenum	64
17	Quantum Yield for Molybdenum	67
18	Normalized Energy Distribution Curves for Molybdenum Plotted Versus $E-\phi$	69
19	Arbitrarily Normalized Energy Distribution Curves of Molybdenum Plotted Versus $E-h\nu$	70
20	Structure Plot for Molybdenum	72
21	Normalized Energy Distribution Curves Multiplied by $(h\nu)n(h\nu)$ of Molybdenum Versus $E-h\nu$	73
22	$N_f^{eff}(E)$ for Various Photon Energies	74
23	Zerth Approximation to the Optical Density of States Used to Estimate the Scattered Electron Contribution to the Energy Distribution Curve of Molybdenum	76
24	Measured, Corrected and Scattered Energy Distribution Curves of Photoemitted Electrons from Molybdenum at $h\nu = 8.0$ eV	78
25	Measured, Corrected and Scattered Energy Distribution Curves of Photoemitted Electrons from Molybdenum at $h\nu = 11.0$ eV	79
26	Optical Density of States of Molybdenum where the Dashed Line is the Average Value for the Density of States above the Fermi Energy	81
27	Reflectance of Ruthenium where i is the Angle of Incidence	84
28	Dielectric Constant of Molybdenum	84
29	Loss Function of Ruthenium	87

List of Figures Continued

Figure		Page
30	Absorption Coefficient α for Ruthenium	87
31	Optical Functions $(h\nu)n(h\nu)$ and $(h\nu)^2 \epsilon_2(h\nu)$ for Ruthenium	88
32	Interband N_{IB} , Surface Plasma N_{sp} , and Volume Plasma N_{vp} Sum Rules for Ruthenium	88
33	Quantum Yield of Ruthenium	91
34	Normalized Energy Distribution Curves of Ruthenium versus $E-h\nu$	93
35	Structure Plot for Ruthenium	94
36	Effective Density of Final States for Ruthenium	97
37	Zeroth Approximation for the Optical Density of States used to Estimate the Scattered Electron Contribution to the Energy Distribution Curves of Ruthenium	98
38	Measured, Corrected and Scattered Energy Distribution of Photoemitted Electrons from Ruthenium at $h\nu = 8.0$ eV	100
39	Measured, Corrected and Scattered Energy Distribution of Photoemitted Electrons from Ruthenium at $h\nu = 11.0$ eV	101
40	Optical Density of States for Ruthenium	103
41	The Optical Density of States of Molybdenum is Shown by the Dashed Line. The Dashed Line Indicates the Density of States Estimated from Matthesis Tungsten (WI) Band Structure Calculations	106

List of Figures Continued

Figure		Page
42	The Optical Density of States from Eastman (1968) (Solid Line) and the Density of States Estimated from Connolly (1968) Band Structure Calculation for Chromium (Dashed Line)	109
43	Comparison of the Optical Density of States of Molybdenum (present study) and Chromium (Eastman, 1968)	111
44	The Optical Density of States of Molybdenum Compared with the Density of States Estimated from Matthesis' Tungsten (W_{II}) Band Structure Calculation. Note the Energy Scale and the Position of the Fermi Level of Matthesis' W_{II} Calculation was Arbitrarily Adjusted	113
45	The Optical Density of States (Solid Line) and the Density of States of Ruthenium Estimated from Matthesis' Rhenium Band Structure Calculation (Dashed Line)	115
46	The Optical Density of States of Ruthenium Compared with the Density of States Estimated from Matthesis' Calculation of the Density of States of Nonmagnetic Iron from Wood's Energy Band Calculations	117
47	Optical Transition Strength Function Calculated from Infrared Optical Constants of Molybdenum Measured by Kirillova et al	123
A-1	Logic Diagram of Computer Program used to Calculate Optical Constants	130
B-1	Quantum Yield of Ruthenium with Approximately Two Monolayers of Cesium	134
B-2	EDC's of Photoemitted Electrons from Cr covered Ru	135

ABSTRACT

The photoemission and optical properties of vapor deposited films of molybdenum (Mo) and ruthenium (Ru) have been measured at room temperature. The photoemission properties measured are in the spectral range of the threshold (4.3 eV and 5.4 eV for Mo and Ru respectively) to 11.8 eV. The optical properties are measured from 0.5 to 11.8 eV. The data from both Mo and Ru are found to be consistent with, and analyzed by, the nondirect transition model. Corrections for the escaping scattered electrons are included in the optical density of states (ODS) analysis. Peaks in the ODS are found at $E - E_F = -0.5$ eV, -1.6 eV, and -3.9 eV for Mo; and -0.4 eV, -1.3 eV, and a third tentatively placed at -3.6 eV for Ru. The ODS for $E > E_F$ is determined by direct numerical inversion of the nondirect model expression for the dielectric constant. Several peaks appear in the ODS of Mo for $E > E_F$ while only one is observed in the ODS of Ru. The ODS of Mo and Ru is compared with the band calculations of Matthesis for tungsten (Matthesis, 1965) and rhenium (Matthesis, 1966) respectively. The relation of the measured ODS's to the explanations based on the electronic density of states for the anomalous isotopic mass dependence of the superconducting transition temperature is discussed. For Mo the volume loss function has a peak at 10.8 eV while the absorption coefficient has a minimum at 11.3 eV, which correlates with a minimum in the quantum yield at approximately 11.0 eV. The energy distribution of the photoemitted electrons show slight structural changes in the spectral range, 10 to 11 eV. In the same spectral region a similar but weaker correlation between structure in the loss function, absorption coefficient, yield, and the energy distributions of Ru is noted.

I. INTRODUCTION

The electronic structure or character of the outer shell electrons determines most of the observed properties of condensed matter. The theory of s- and d-like outer shell electrons in the transition metals has been investigated by detailed band structure calculations within the one-electron or independent particle approximation. These calculations are now possible largely because of the availability of high-speed computers. Much experimental work on the electrons in metals has been done by methods such as de Haas-van Alphen, cyclotron resonance, magnetoacoustic, high field magnetoresistance, and anomalous skin effect measurements. These measurements only probe the state in the immediate vicinity of the Fermi energy. Electronic states below the Fermi energy may be investigated by soft x-ray absorption and emission, and Auger electron emission produced by ion bombardment. The latter two methods are capable of giving information concerning the gross features of the occupied outer shell or valence electronic structure, but lack sufficient resolution to yield detailed information that can be compared with the theoretical results.

The band structure calculations for the transition and noble metals indicate the electronic structure of these metals is on the order of 10 eV wide. This energy range is

investigated conveniently by photoemission and optical studies using vacuum ultraviolet radiation. Detailed experimental information concerning the outer shell electrons for the noble metals over a wide range of energy was first demonstrated by the optical investigations of Ehrenreich and Philipp (1962). Their results were correlated with detailed band calculations by assuming conservation of the Bloch state wave vector, \vec{k} , in the optical excitation process. Shortly afterwards, Berglund and Spicer (1964) demonstrated that more detailed correlations could be obtained between band structure predictions and experimental photoemission observations in the metals copper (Cu) and silver (Ag), provided conservation of the Bloch wave number, or crystal momentum selection rule, was ignored for emission from d-like states. The model of Spicer and Berglund was called the nondirect model in contrast with the standard Bloch wave-number-conserving direct transition model. The subsequent investigation of Spicer and his co-workers soon produced results which indicated nondirect transitions were dominant in the photoemission data of the 3d transition metals nickel (Ni), iron (Fe) (Blodgett and Spicer, 1967), and cobalt (Co) (Yu and Spicer, 1967). These results were extended to the 3d metal chromium (Cr) by Lapeyre and Kress (1968). The 3d metal Mn was completed and the whole 3d series reinvestigated by Eastman (1969). Before the nondirect

optical transition model could be associated with the d-band structure of metals in general, it became apparent that the systematics of the electronic structure in the 4d and/or 5d transition metals should be investigated.

Photoemission and optical investigations of the density of states of the 4d and 5d transition metals could also give information on the validity of the rigid band model. In its simplest form the rigid band model for a given transition metal period (e.g. the 3d period vanadium (V), Cr, manganese (Mn), etc.) predicts only the position of the Fermi energy and not the structure changes in the density of states as one proceeds across the periodic table. Furthermore, for a given group (e.g. group VI B: Cr, molybdenum (Mo), and tungsten (W)), neither the position of the Fermi energy nor the structure of the density of states should change according to the rigid band model. The details of these predictions are expected to fail when the crystal structure of the adjacent metals changes.

The transition metals have an anomalous isotopic mass dependence in their superconducting transition temperatures (Garland, 1963). In particular the 4d transition metals ruthenium (Ru) and Mo deviate from the normal isotopic mass effect observed in simple metals. The 4d transition metals Ru and Mo were chosen for this investigation to add further knowledge to the systematics of the electronic structure of

the transition metals beyond the 3d series and to investigate possible anomalous structure in the d-bands which could account for their superconducting transition temperatures.

II. PHOTOEMISSION AND OPTICAL PROPERTIES OF METALS

Measurements of the kinetic energy distribution of photoemitted electrons as a function of the incident photon energy constitute the greatest single source of information obtained from photoemission experiments. The energy distribution curves (EDC's) of the photoemitted electrons from a metal may be related to the electronic structure of the photoemitting material according to the following simplified model. The photoemission process may be separated conceptually into three stages: photoexcitation of the electron by atomic absorption of the incident photon, transport of the excited electron through the solid, and escape across the surface boundary of the metal. The incident photons transmitted through the surface of the metal are typically absorbed within a few hundred Angstroms of the surface. The excited electrons produced by the photon absorptions can escape the metal provided they have the proper momentum and have kinetic energies greater than the vacuum level, i.e. the Fermi energy plus the photoelectric work function. During transport of the excited electrons towards the surface, nearly elastic (e.g. electron-phonon) and inelastic (e.g. electron-electron) collisions may take place. Estimates of the mean inelastic scattering lengths for the photoexcited electrons in

transition metals are a few tens of Angstroms (Eastman, 1968). Finally, the electrons will escape the metal provided their component of momentum perpendicular to the surface is sufficient to overcome the photoelectric work function.

If transport and surface escape effects of the photoemitted electrons can be neglected or properly handled, the kinetic energy of the photoelectrons is simply related to its initial and final energy by the conservation of energy principle. From the above model, the EDC's of photoemitted electrons as a function of photon energy are related to the relative transition probability between the initial and final states. The experimental transition probability can then be directly related to the electronic structure or density of states at initial and final energy.

Measurements of the reflectance as a function of the incident photon energy may also be used to obtain information about the electronic structure. The optical "constants" derived from the measured reflectance as a function of the photon energy, $E = h\nu$ can be related to the total optical transition probability of all states separated by the energy $h\nu$. The energy of the photoexcited electron produced by photon absorption is not determined by optical studies, therefore the absolute energy of the initial or final states participating in the transitions cannot be determined. Since

the optical constants are directly related to the sum of all optical transitions which conserve energy, they provide less precise information about electronic structure of metals than photoemission functions.

When both photoemission and optical studies are performed on the same metal, there is sufficient complementarity and overlap of the data to allow checks and extensions of the information obtained. Photoemission and optical studies are combined in the present study to produce a more comprehensive study of the electronic structure of metals.

A. Optical Constants

Beginning with Maxwell's equations and the constitutive equations, the interaction of radiation with matter can be described by a set of optical "constants" which vary with the photon energy. There are three sets of complex optical constants generally defined in optical measurements. Any one of these sets is equivalent to any other set. These constants are the complex refractive index $N(h\nu)$, complex dielectric constant $\epsilon(h\nu)$ and complex conductivity $\sigma(h\nu)$ where, in cgs units:

$$N(h\nu) = n(h\nu) + ik(h\nu), \quad (2-1)$$

$$\epsilon(h\nu) = \epsilon_1(h\nu) + i \epsilon_2(h\nu), \quad (2-2)$$

and

$$\sigma(h\nu) = \sigma_1(h\nu) + i \sigma_2(h\nu). \quad (2-3)$$

With the aid of Maxwell's equations and the constitutive equations, these constants may be related to each other (Pines, 1964)

$$N^2(h\nu) = \epsilon(h\nu) = 1 + \frac{2i \sigma(h\nu)}{\nu} \quad (2-4)$$

The real and imaginary parts of this equation can be set equal and relationships between these portions derived,

$$\epsilon_1(h\nu) = n^2(h\nu) - k^2(h\nu) = 1 - 2 \sigma_2/\nu \quad (2-5)$$

and

$$\epsilon_2(h\nu) = 2n(h\nu) k(h\nu) = 2 \sigma_1/\nu \quad (2-6)$$

Another optical constant that is considered is the absorption coefficient $\alpha(h\nu)$. The absorption coefficient is defined as the light intensity change per unit distance per unit intensity and is simply related to $k(h\nu)$ by

$$\alpha(h\nu) = \frac{4\pi k(h\nu)}{\lambda} \quad (2-7)$$

where λ is the wavelength of the incident radiation.

The imaginary part of the dielectric constant, $\epsilon_2(h\nu)$, is directly related to the total optical absorption probability. The relation between $\epsilon_2(h\nu)$ and the total number of optical excitations has been derived by Berglund and Spicer (1964).

Assuming monochromatic incident radiation and the correspondence principle their derivations shows that the total number of transitions per second is proportional to ϵ_2 multiplied by the photon energy squared, i.e.

$$(\hbar\nu)^2 \epsilon_2(\hbar\nu) \propto \int_0^{\hbar\nu} P_{if} dE \quad (2-8)$$

where P_{if} is the rate of transitions of electrons initially with energy $E-\hbar\nu$ to energy E and the zero of the energy scale is at the highest energy of the occupied levels. Using the explicit expression for P_{if} developed later for the nondirect transition model (cf Eq. (2-19)), the above equation may be written as

$$(\hbar\nu)^2 \epsilon_2(\hbar\nu) = A \int_0^{\hbar\nu} N_i^{\text{opt}}(E-\hbar\nu) N_f^{\text{opt}}(E) dE \quad (2-9)$$

where A is a constant and N_i^{opt} and N_f^{opt} are the optical density of initial and final states respectively. The optical function $(\hbar\nu)^2 \epsilon_2(\hbar\nu)$ will be called the optical transition strength function and is important in the determination of $N_f^{\text{opt}}(E)$.

The optical dielectric constant $\epsilon(\hbar\nu)$ can be used to determine the photon energy at which the properties of the metal deviate from free electron-like behavior. For example, Ehrenreich and Philipp (1962) have shown that

$$\epsilon(h\nu) = \epsilon_f(h\nu) + \epsilon_i(h\nu) , \quad (2-10)$$

where $\epsilon_i(h\nu)$ represents the interband transitions and $\epsilon_f(h\nu)$ represents intraband transitions. The intraband portion has the same form as results from the classical Lorentz model for electrons in a metal, i.e.

$$\epsilon_f(h\nu) = 1 - \frac{v_p^2}{[m\nu(\nu + \frac{i}{\tau})]} , \quad (2-11)$$

where $v_p^2 = 2Ne^2/m$, $N = \text{electrons/volume}$, m is the mass of the electron, and $m/\tau = \text{effective damping constant}$. The real part of the free electron-like portion of the dielectric constant, $\epsilon_f(h\nu)$, monotonically approaches unity while the imaginary part falls monotonically to zero as ν increases.

The energy of collective excitations may be determined from the optical constants. It has been shown that the general condition for a plasma oscillation at frequency Ω is $\epsilon(\Omega) = 0$ (Pines, 1964). This condition yields $\Omega = \omega_p + i\Gamma$ where ω_p is the plasma frequency and Γ describes the damping. When there is little damping, or $\epsilon_2(\omega_p) \approx 0$, the condition for plasma resonance becomes $\epsilon_1(\omega_p) = 1$. Then $\text{Im } 1/\epsilon$, the volume loss function approaches a peak value of $1/\epsilon_2(\omega_p)$ at ω_p . In general, a plasma resonance can be distinguished from interband effects which can also produce structure in $\text{Im } 1/\epsilon$ by noting that in the former case, both ϵ_1 and ϵ_2 are small near

the maximum in the loss function and have a positive and negative slope respectively (Philipp, 1965). A similar statement may be made concerning peaks in the surface plasma loss function $\text{Im } 1/(\epsilon + 1)$ correlating with the surface plasma excitations (Ritchie, 1967).

Several sum rules are associated with the optical constants. Three such sum rules which define the effective number of electrons per atom participating in interband transition, volume plasmon (Nozieres and Pines, 1959), and surface plasmon excitations (Ritchie, 1968) below the energy $h\nu$ are given respectively by

$$N_{IB}(h\nu) = \frac{m}{2\pi^2 N e^2 \hbar^2} \int_0^{h\nu} \epsilon_2(E) E dE, \quad (2-12)$$

$$N_{VP}(h\nu) = \frac{m}{2\pi^2 N e^2 \hbar^2} \int_0^{h\nu} [-\text{Im}(1/\epsilon(E))] E dE, \quad (2-13)$$

and

$$N_{SP}(h\nu) = \frac{2m}{\pi^2 N e^2 \hbar^2} \int_0^{h\nu} [-\text{Im}(\frac{1}{\epsilon(E)+1})] E dE \quad (2-14)$$

where m is the free electron mass and N is the number of atoms per unit volume.

B. Photoemission

The results of the present photoemission study are found to be consistent with and will be analyzed by the nondirect optical transition model (Berglund and Spicer, 1964). Other

models for optical transition in solids have been proposed (a review of two other models is given by Berglund, 1964) but have predicted different effects than those observed in the present investigation. Only key results relevant to the nondirect model and the interpretation of the present study will be presented here. The reader is referred to the cited references for expanded discussions and more detailed derivations.

1. Photoexcitation. The photoemission properties of a metal may be interpreted in terms of its electronic structure by considering specific models for the three stages of photoemission of electrons outlined above. In the nondirect model, the initial photoexcitation process is treated by an application of first order time dependent perturbation theory. If the electrons in a metal are perturbed by a weak, long wavelength (compared to atomic dimensions), electromagnetic field, the perturbing Hamiltonian is given by

$$H' = e/2mc \sum_i \vec{p}_i \cdot \vec{A}(\vec{r}_i) \quad (2-15)$$

where \vec{p}_i is the momentum operator of the i^{th} electron and $\vec{A}(\vec{r}_i)$ is the vector potential of the perturbing radiation field. In metals the occupied initial states and unoccupied final states of the electron (sometimes called valence and conduction states respectively) are quasi-continuous with

energy as displayed in Fig. 1. Hence, summing over the

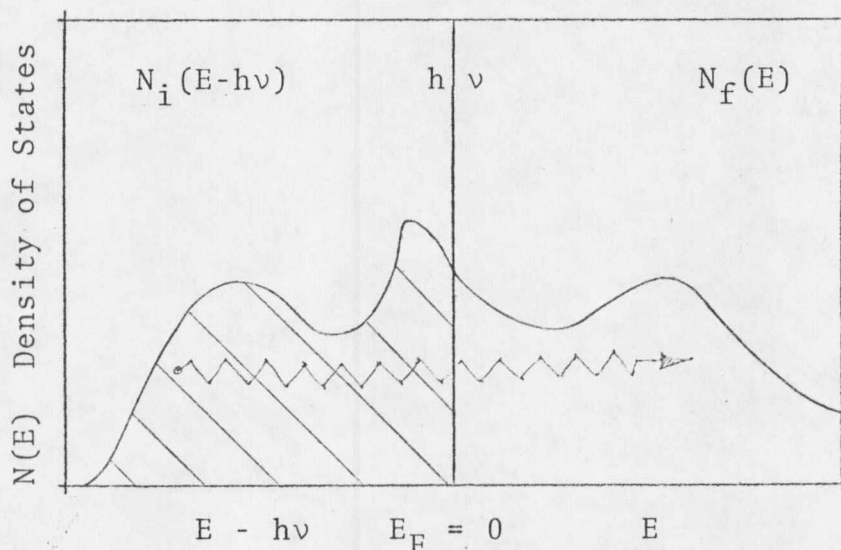


Fig. 1. Hypothetical Density of States for a Transition Metal. Shaded Area Represents Occupied or Initial States and Open Area Represents Unoccupied or Final States.

initial states, assumed distributed with a density N_i per unit energy, and explicitly putting in energy conservation, i.e. $E_f = E$ and $E_i = E - h\nu$ (the zero of the energy scales is assumed to be the Fermi energy as shown in Fig. 1), the standard perturbation theory result for the rate of transitions from energy $E - h\nu$ to E (Messiah, 1962) is

$$P_{if} = \frac{2\pi}{\hbar} \left| \langle \Psi_f | H' | \Psi_i \rangle \right|^2 N_i(E-h\nu) N_f(E) \quad (2-16)$$

$$= M^2 N_i(E-h\nu) N_f(E) \quad (2-17)$$

where $N_i(E-h\nu)$ is the density of initial states at energy $E - h\nu$, $N_f(E)$ is the density of final states at energy E , Ψ_i and Ψ_f are the exact initial and final states wave functions respectively, and the matrix element is abbreviated as M^2 . From Eq. (2-17) it is seen that to first order the number of photoexcited electrons to energy E depends upon three factors: a matrix element, M^2 , the density of final states, $N_f(E)$, and the density of initial states, $N_i(E-h\nu)$.

It is difficult to obtain a theoretical expression for the matrix element, M^2 , since the exact ground state and excited state wave functions are unknown. The matrix elements contain all the selection rules determined by the symmetry and spin states of the exact initial and final state wave functions coupled by the interaction Hamiltonian and was expected to be rapidly varying with respect to energy. Contrary to this expectation, the initial experimental results (Berglund and Spicer, 1964) indicated that M^2 could be treated as if it was nearly constant. It was later realized that if the matrix element was proportional to a product of functions which depend on the initial and final state energy of the

electrons, $E - h\nu$ and E respectively, variations of the matrix elements could not be distinguished from the effects due to unperturbed ground state density of states (Spicer, 1967). This assertion becomes clear if the postulated matrix element dependence is substituted into Eq. (2-17).

$$P_{if}(E, E-h\nu) = M_i(E-h\nu)N_i(E-h\nu)M_f(E)N_f(E) \quad (2-18)$$

$$= B N_i^{\text{opt}}(E-h\nu)N_f^{\text{opt}}(E) \quad (2-19)$$

where B is proportional to the photon flux and the definition

$$N_i^{\text{opt}}(E-h\nu) = M_i(E-h\nu)N_i(E-h\nu) \quad (2-20)$$

and

$$N_f^{\text{opt}}(E) = M_f(E)N_f(E) \quad (2-21)$$

have been used.

The experimentally observable densities of states $N_i^{\text{opt}}(E-h\nu)$ and $N_f^{\text{opt}}(E)$ are called the optical density of initial and final states respectively. Spicer (1967) has postulated the optical density of states (ODS) may differ from the ground state density of states (DS) due to relaxation effects that occur during optical excitation. Others have estimated matrix element variations due to the character of the d-band wave function (Cuthill et al., 1967). Optical and/or photoemission investigations study the optical transition probability and do not study the matrix elements directly. Effects due to the

ground state density of states and those due to matrix element variations cannot be unambiguously distinguished by optical excitation.

2. Transport and Escape. The transport of the photoexcited electrons in a metal may be approximately treated by assuming that the number of electrons excited at a depth x below the surface of the metal is proportional to the absorbed light intensity $\alpha(h\nu)e^{-\alpha(h\nu)x}$ at x . The subsequent probability of the photoexcited electron reaching the surface without scattering is further assumed to be proportional to $e^{-x/L(E)}$ where $L(E)$ is the energy dependent, mean scattering length of the excited electrons with energy E (Berglund and Spicer, 1964). Averaging these effects over all depths x , the total probability of a photoexcited electron with energy E migrating to the surface of the metal without being scattered is proportional to

$$P_t \propto \alpha(h\nu) \int_0^{\infty} e^{-\alpha(h\nu)x} e^{-x/L(E)} dx \quad (2-22)$$

$$= \frac{\alpha(h\nu) L(E)}{1 + \alpha(h\nu) L(E)} \quad (2-23)$$

$L(E)$ is the effective escape length and will become degenerate with the electron-electron scattering length in the approximate treatment assumed in the following development.

If the above derivation is done for a three dimensional solid, a function $K(\alpha, L, T)$ appears as a factor in the

transport term (Berglund and Spicer, 1964). K is a very slowly varying function and is bound between 0.5 and 1.0 for all α , L , and T . This factor will be neglected in the present study.

The probability of the excited electrons escaping across the surface boundary of the metal into the vacuum is treated in the calculation of the threshold function, T . In general T is a complex function of the bulk and surface properties of the metal and is dependent on the details of the scattering mechanisms (Stuart and Wooten, 1967). Insight into the effects of the threshold function can be gained by considering the threshold function derived for classical noninteracting electrons with energy E and isotropic velocity distribution in a step potential well of depth ϕ (Berglund and Spicer, 1964),

$$T_f(E) = \begin{cases} 0 & E < \phi & (2-24) \\ \frac{1}{2}(1 - \sqrt{\phi/E}) & E \geq \phi & (2-25) \end{cases}$$

It is apparent from Fig. 2 that electrons with energy less than ϕ , the photoelectric work function, will not escape the metal. $T_f(E)$ is a monotonically increasing function for $E > \phi$ and is most rapidly varying for $E \approx \phi$.

3. Photoemitted Electrons. An expression for the number of electrons photoemitted from the metal is obtained by multiplying the probability of transport and escape of the

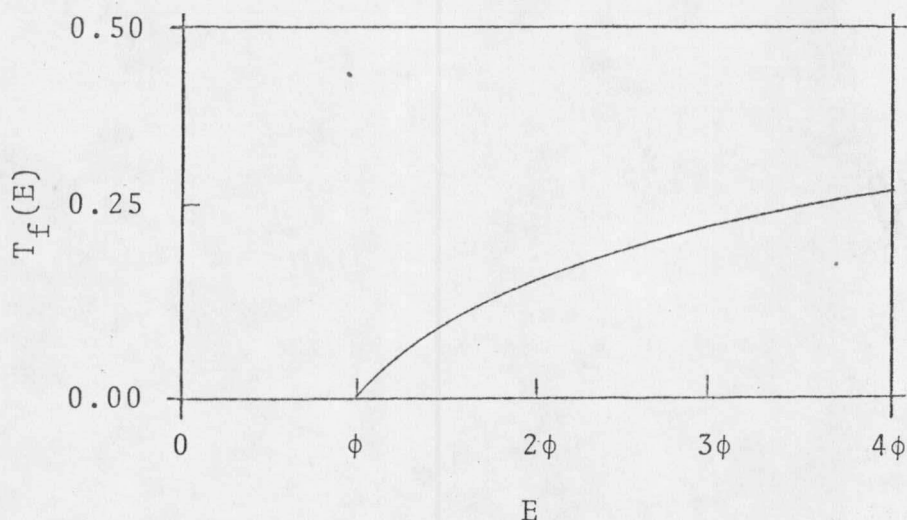


Fig. 2. Free Electron Threshold Function in Units of the Photoelectric Work Function, ϕ .

electrons by their probability of excitation, or

$$N(E-\phi, h\nu) \propto \frac{T\alpha(h\nu)L(E)N_i^{\text{opt}}(E-h\nu)N_f^{\text{opt}}(E)}{1 + \alpha(h\nu)L(E)}, \quad (2-26)$$

where the energy argument of the photoemitted electrons is now $E - \phi$ since the electrons lose the energy ϕ escaping from the metal.

It is useful to normalize the above expression for photoemitted EDC's to the total number of photoexcited electrons/absorbed photons. The total number of photoexcited electrons/absorbed photons is proportional to the optical transition strength function (cf Eq. (2-8)) and the normalized

$$N(E-\phi, h\nu) = \frac{A T \alpha(h\nu) L(E) N_i^{\text{opt}}(E-h\nu) N_f^{\text{opt}}(E)}{[1 + \alpha(h\nu) L(E)] (h\nu)^2 \epsilon_2(h\nu)}, \quad (2-27)$$

where A is a constant. Since the optical transition strength is an experimentally measured quantity, the effects of the exact matrix element are included in the normalization.

4. Quantum Yield. The absolute quantum yield of the metal is defined as the number of photoemitted electrons per absorbed photon. Using the expression for the normalized EDC, the yield is the sum of all the photoemitted electrons normalized to the total number of photoexcited electrons or

$$Y(h\nu) = \int_{\phi}^{h\nu} N(E-\phi, h\nu) dE \quad (2-28)$$

5. Scattered Electrons in the Energy Distribution Curves. Multiple nearly elastic electron-phonon and inelastic electron-electron scattering events of photoexcited electrons have been considered by detailed Monte Carol calculations (Stuart and Wooten, 1967). These calculations were done assuming an isotropic velocity distribution of the photoexcited and scattered electrons in addition to energy dependent mean scattering lengths. The multiple scattering calculations indicate that the effects of the elastic scattering events may be summarized in the threshold function so that $T \approx T(E)$.

The multiple scattering calculations also indicate that inelastic scattering events which result in energy losses of several eV per collision produce the dominant observable effects on the EDC's. Since the photoelectric work functions are typically several eV and the photon energy is limited by the spectral transmission of the window on the experimental chamber, only a small fraction of the electrons which are scattered possess sufficient energy to escape the metal. The scattered electrons which do manage to escape the metal will be called secondaries.

An approximate analytical expression for photoemitted once scattered secondary electrons has been developed (Berglund and Spicer, 1964). This analytical expression was found to be an adequate description of scattering processes in a metal by the more eloquent Monte Carlo multiple scattering calculations of Stuart and Wooten (1967) for all but the lowest energy photoemitted electrons. Since the analytical expression for secondaries has been shown to be a reasonable approximation, it will be used for the analysis of the measurements performed in the present study.

The analytical expression of Berglund and Spicer for escaping scattered photoexcited electrons is derived by assuming only inelastic electron-electron scattering events are significant. The desired expression is obtained by

considering the scattering event pictured in Fig. 3.

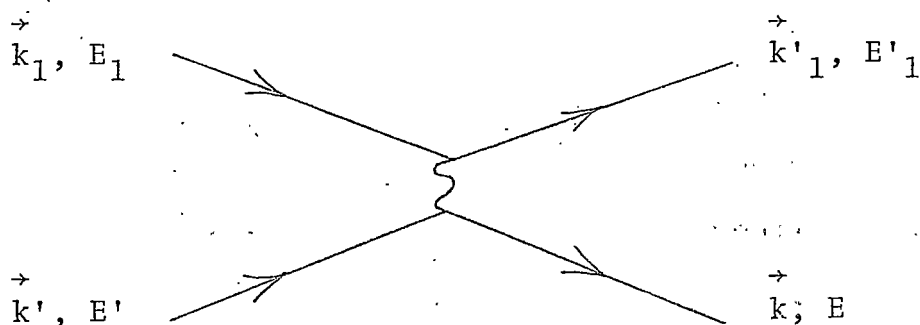


Fig. 3. Electron-Electron Scattering Event.

If constant matrix elements are assumed, the probability of the electron-electron event may be calculated by finding the overlapping phase space for all \vec{k}_1 , \vec{k}'_1 , \vec{k} , and \vec{k}' in the standard manner. Assuming further, the scattered electrons have an isotropic velocity distribution, $\alpha(h\nu)L(E) \ll 1$ and $L(E)/L(E') \ll 1$ if $E' > E$, the expression for the energy distribution of the photoemitted electrons is modified by the inclusion of a small term containing the electron-electron scattering probability, i.e. Eq. (2-27) becomes

$$N(E-\phi, h\nu) = \frac{A T(E)\alpha(h\nu)L(E)N_i^{\text{opt}}(E-h\nu)N_f^{\text{opt}}(E)}{[1 + \alpha(h\nu)L(E)](h\nu)^2 \epsilon_2(h\nu)} \times \left[1 + \frac{2 \int_0^{h\nu} \frac{P(E, E') N_i^{\text{opt}}(E'-h\nu) N_f^{\text{opt}}(E') dE'}{P(E')}}{N_i^{\text{opt}}(E-h\nu) N_f^{\text{opt}}(E)} \right] \quad (2-29)$$

$$= S_0(E, h\nu) N_i^{\text{opt}}(E-h\nu) N_f^{\text{opt}}(E) [1 + S_i(E, h\nu)] \quad (2-30)$$

where

$$P(E, E') = N_f^{\text{opt}}(E) \int_{-(E'-E)}^0 N_i^{\text{opt}}(E_1) N_f^{\text{opt}}(E_1 + E' - E) dE_1 \quad (2-31)$$

$$P(E') = \int_0^{E'} P(E, E') dE \quad (2-32)$$

$$S_0(E, h\nu) = \frac{A T(E)\alpha(h\nu)L(E)}{1 + \alpha(h\nu)L(E)} \quad (2-33)$$

$$S_i(E, h\nu) = \frac{2 \int_0^{h\nu} \frac{P(E, E') N_i^{\text{opt}}(E'-h\nu) N_f^{\text{opt}}(E') dE'}{N_i^{\text{opt}}(E-h\nu) N_f^{\text{opt}}(E)} \quad (2-34)$$

One notable property of Eq. (2-30) is that the fraction of scattered electrons at energy E is independent of the mean scattering length and is given by

$$\text{fraction scattered} = \frac{S_i(E, h\nu)}{1 + S_i(E, h\nu)} \quad (2-35)$$

Equation (2-34) indicates that $S_i(E, hv) \rightarrow 0$ as $E \rightarrow hv$, that is, the fraction of scattered electrons becomes smaller for the higher energy portions of the EDC's.

C. Optical Density of States Analysis

The central analysis problem is to obtain the ODS from the experimentally determined EDC's. The ODS analysis procedure developed in the present study for determination of the density of states below the Fermi energy is a combination of methods used by Lapeyre and Kress (1968) and Eden (1967). The above methods were extended to include an estimate of the effects of secondaries in the EDC's. The explicit computational procedure developed for determining the density of states above the Fermi energy is unique to the present study but is a direct extension of the implicit computations used by others (Berglund and Spicer, 1964). The following procedure unambiguously locates the structure in the ODS but can only approximately determine the magnitude of the ODS due to the secondaries and experimental uncertainties.

The ODS analysis simplifies in two limiting cases where the transport factor becomes

$$\frac{\alpha(h\nu)L(E)}{1 + \alpha(h\nu)L(E)} = \begin{cases} 1, & \alpha L \gg 1 \\ \alpha L, & \alpha L \ll 1 \end{cases} \quad \begin{matrix} \text{(Case 1)} \\ \text{(Case 2)} \end{matrix} \quad \begin{matrix} (2-36) \\ (2-37) \end{matrix}$$

For Case 1, the expression for the normalized EDC is given by

$$N(E-\phi, h\nu) = \frac{AT(E)N_i^{\text{opt}}(E-h\nu)N_f^{\text{opt}}(E)[1+S_i(E-h\nu)]}{(h\nu)^2 \epsilon_2(h\nu)} \quad (2-38)$$

$$= \frac{AN_i^{\text{opt}}(E-h\nu)N_f^{\text{eff}}(E)[1+S_i(E, h\nu)]}{(h\nu)^2 \epsilon_2(h\nu)} \quad (2-39)$$

where the functions that vary as E have been summarized as $N_f^{\text{eff}}(E)$. The limit $\alpha(h\nu)L(E) \gg 1$, implies that the mean scattering length is large compared to the mean absorption depth. With little scattering most of the photoexcited electrons should escape and the quantum yield per absorbed photon should be large.

Contrary to the above prediction, the observed quantum yields of molybdenum, ruthenium and other transition metals are typically .01 to .02 photoemitted electrons/absorbed photon for $E \lesssim 12$ eV (cf. Yu and Spicer, 1967). The small values observed for the quantum yield implies the opposite limit, $\alpha(h\nu)L(E) \ll 1$, where most of the electrons are scattered and consequently do not escape. In this limit which is appropriate for transition metals, Eq. (2-30) becomes

$$N(E-\phi, h\nu) = \frac{AT(E)\alpha(h\nu)L(E)N_i^{\text{opt}}(E-h\nu)N_f^{\text{opt}}(E)[1+S_i(E, h\nu)]}{(h\nu)^2 \epsilon_2(h\nu)} \quad (2-40)$$

$$= \frac{AN_i^{\text{opt}}(E-h\nu)N_f^{\text{eff}}(E)[1+S_i(E, h\nu)]}{(h\nu)n(h\nu)} \quad (2-41)$$

where Eq. (2-1) and Eq. (2-2) have been used and all functions that vary as E have been summarized as $N_f^{\text{eff}}(E)$. Only the $\alpha L \ll 1$ limit is considered in the following treatment since the quantum yields of the metals investigated in the present study are small for the highest photon energies.

The character of the optical transitions are found to be consistent with the nondirect model and the position of structure in the ODS is determined by simple procedures provided the contribution of secondaries is small. In the present study there are few secondaries in the EDC's for all but the highest photon energies (Chapter IV and V). If there are few secondaries $S_i(E, h\nu)$ is small and Eq. (2-41) reduces to

$$N(E-\phi, h\nu) = \frac{AN_i^{\text{opt}}(E-h\nu)N_f^{\text{eff}}(E)}{(h\nu)n(h\nu)} \quad (2-42)$$

It is apparent from Eq. (2-42) that if the EDC's are plotted as a function of $E - h\nu$ the structure in the EDC's due to N_f^{opt} moves by an equal energy increment $\Delta(h\nu)$ if $h\nu \rightarrow h\nu + \Delta(h\nu)$ while that due to N_i^{eff} remains fixed. This

rule, called the equal increment rule, is conveniently tested for all the EDC's over a wide range of photon energies by plotting the energy position of the observed structure versus photon energy as shown in the hypothetical case presented in Fig. 4. The structures labeled 1 and 2 in Fig. 4 are identified with the structure in N_i^{opt} and N_f^{eff} , respectively. The structure labeled 3 is not consistent with the nondirect transition model.

A continuous estimate of N_i^{opt} between the structure points is found by including the effects of the secondaries in the ODS analysis method proposed by Eden (1967). Consider two energies in the optical density of initial states at ξ_1 and ξ_2 . Choose E, hv_1 , and hv_2 such that $\xi_1 = E - hv_1$ and $\xi_2 = E - hv_2$. The relative amplitude of the density of initial states at ξ_1 and ξ_2 is then found from Eq. (2-41) to be

$$\frac{N_i^{\text{opt}}(\xi_1)}{N_i^{\text{opt}}(\xi_2)} = \frac{N(E-\phi, hv_1)(hv_2)n(hv_2)[1+S_i(E, hv_1)]}{N(E-\phi, hv_2)(hv_1)n(hv_1)[1+S_i(E, hv_2)]} \quad (2-43)$$

In all generality, $1+S_i(E, hv)$ must be known before $N_i^{\text{opt}}(\xi_1)$ relative to $N_i^{\text{opt}}(\xi_2)$ may be determined. $S_i(E, hv)$ is a functional of the optical density of states, N_i^{opt} and N_f^{opt} (Eq. 2-34). Fortunately, $S_i(E, hv)$ is not a strong functional of the details of N_f^{opt} since they determine $S_i(E, hv)$ through an integral relation.

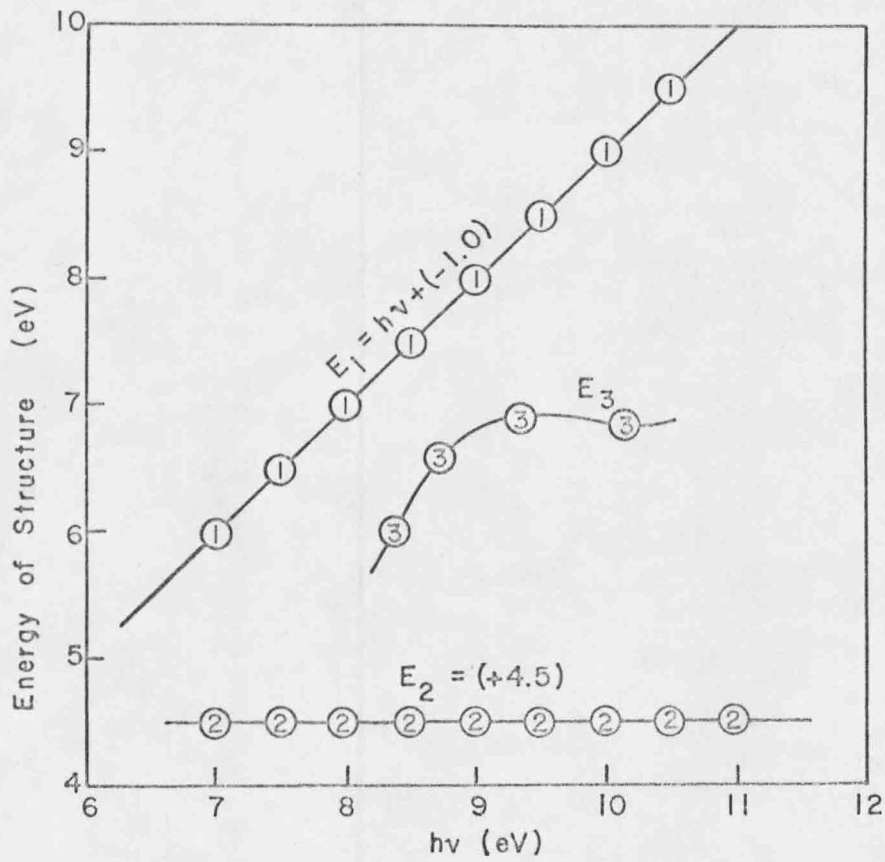


Fig. 4 . Hypothetical EDC Structure Plot

Since the ODS enters the scattering expression $S_i(E, h\nu)$ in an insensitive manner, an approximate ODS will suffice for a reasonable estimate of the scattering effects. The zeroth approximation to the optical density of initial states, $N_{i0}^{opt}(E-h\nu)$, is found by the technique used by Lapeyre and Kress (1968) and Yu and Spicer (1967) to arrive at their final results. Their method is based on Eq. (2-42) and the assumption that $N_f^{eff}(E) = T(E)L(E)N_f^{opt}(E)$ remains relatively constant over a small energy interval in the range $E = \phi + 1.5$ eV to $E = \phi + 3.0$ eV. Assuming N_f^{eff} approximately constant, the zeroth approximation to the shape of $N_i^{opt}(E-h\nu)$ is found by choosing the shape of the experimental EDC's at 1.5 to 3.0 eV above the threshold energy. This is conveniently done from log plots of the EDC's where normalization and $h\nu$ dependence in general can be ignored. The relative amplitude of various points in $N_{i0}^{opt}(E-h\nu)$ is made unique within the experimental error and the error produced by $S_i(E, h\nu)$ by use of Eq. (2-41) (see Krolikowski (1967) for complete discussion of the uniqueness problem). $N_f^{eff}(E)$ is then obtained by dividing $N_{i0}^{opt}(E, h\nu)$ into the EDC's at various photon energies. Provided the resultant effective density of final states, N_f^{eff} , is similar for all photon energies, the technique is assumed to yield a reasonable approximation to N_i^{opt} .

In principle the above technique may be used to estimate

the density of initial states for $E \gtrsim \phi - 11.9$ eV since the photon energy is limited to $h\nu \lesssim 11.9$ eV by the LiF window transmission. In practice the threshold function and scattered electrons severely distort the lower 2 eV portion of the highest photon energy EDC's imposing a more practical limit of $E \gtrsim \phi - 9.9$ eV. The shape of the highest photon energy EDC was used as a guide to determine the low energy cut-off of the density of initial states. The resultant cut-off is too slow for the zeroth approximation because of secondaries but is corrected in the next approximation where the secondaries are eliminated from the EDC's.

The density of final states above the Fermi energy, N_f^{opt} , is determined from the density of initial states below the Fermi energy using the measured optical transition function and the optical transition strength integral (Eq. 2-8). Previous investigators (e.g. Berglund and Spicer, 1964) determined N_f^{opt} by an implicit calculation. N_i^{opt} was determined as indicated above, the form of N_f^{opt} estimated, and Eq. (2-8) computed. After comparing the resultant shape of the calculated optical transition strength function with the measured value, $N_f^{\text{opt}}(E)$ was adjusted until satisfactory agreement was obtained.

A more direct approach is taken in the present study. Given either N_{i0}^{opt} or N_i^{opt} and the numerical values of the measured optical transition strength function, Eq. (2-9) is

numerically inverted to find N_{fo}^{opt} or N_f^{opt} respectively. This numerical inversion is done from finite difference approximation for the integral expression in Eq. (2-9), i.e.

$$L = \frac{h\nu}{E} = M$$

$$(M\Delta E)^2 \epsilon_2(M\Delta E) \approx A \sum_{L=1} N_i^{opt} [(L-M-1)\Delta E] N_f^{opt} [(L-1)\Delta E] \Delta E \quad (2-44)$$

where the energy scale has been divided into equal increments of width ΔE and $h\nu = M\Delta E$. The constant A is determined since by assuming $M = 1$ and rearranging Eq. (2-44) gives

$$A \approx \frac{(\Delta E)^2 \epsilon_2(\Delta E)}{N_i^{opt}(\Delta E) N_F \Delta E} \quad (2-45)$$

where the continuity of the density of states function was used, i.e. $N_f^{opt}(0) = N_F =$ density of states at the Fermi energy, and all other quantities on the right side of Eq. (2-45) are known.

With A and $N_f^{opt}(0)$ determined, it will be shown that $N_f^{opt}[(M-1)\Delta E]$ is determined for all energies where N_i^{opt} and the optical transition functions are known. Then by induction N_f^{opt} is determined for all $E < (M-1) E$. The desired result is obtained by considering only the $L = M$ term in Eq. (2-41) and solving for N_f^{opt} , i.e.

$$N_f^{\text{opt}}[(M-1)\Delta E] \approx \frac{1}{AN_F\Delta E} \left\{ (M\Delta E)^2 \epsilon_2(M\Delta E) - \right. \\ \left. A\Delta E \sum_{L=1}^{M-1} N_i^{\text{opt}}[(L-M-1)\Delta E] N_f^{\text{opt}}[(L-1)\Delta E] \right\} \quad (2-46)$$

Since the cut-off assumed for N_{i0}^{opt} was rather uncertain, the zeroth approximation for N_{fo}^{opt} , was determined from the above calculation only for $E \lesssim 9.9 \text{ eV} - \phi$. N_{fo}^{opt} was extended beyond this energy by assuming a free electron density of states.

The final estimate of the ODS is obtained from the EDC's corrected for secondaries. The contribution of the secondaries in the EDC's at various photon energies is estimated by the calculation of Eq. (2-38) using the zeroth approximation to the ODS extended to $|E| \lesssim 12 \text{ eV}$ as described above. The estimated fraction of secondaries was subtracted from the EDC's to obtain a set of corrected EDC's. With this set of corrected EDC's available, a slight rearrangement of Eq. (2-43) is used to help define N_i^{opt} . In the present study a combination of the analysis used by Lapeyre and Kress (1968) and Eq. (2-43) was used to obtain the final estimate of N_i^{opt} . The combination of analysis techniques was necessary because of experimental uncertainties in the yield and possible collective effects in the optical constants for $h\nu \gtrsim 10 \text{ eV}$. The final estimate for N_f^{opt} was obtained by again inverting the optical

transition strength relation (Eq. 2-46) using the final estimate of N_i^{opt} . No further iteration of the ODS analysis was deemed reasonable considering the assumption and approximation involved in the scattering correction.

D. Summary

An expression for the EDC's of photoemitted electrons has been obtained including a correction for once scattered electrons. The expression has been derived from the nondirect transition model (i.e. conservation of Bloch wave number is not a good selection rule) and the following assumptions:

1. The initial velocity distribution of excited electrons is isotropic.
2. Only inelastic scattering events need be considered.
3. The probability of inelastic scattering can be described in terms of a mean free path which is a function of the electron energy.
4. The inelastic scattering is isotropic.
5. The electron must have a component of its total crystal momentum P , perpendicular to the surface, greater than some critical value.
6. For the transition metals studied $\alpha(h\nu)L(E) \ll 1$ and $L(E')/L(E) \ll 1$ if $E' < E$.

An implicit assumption of the above model is that many-body effects are negligible. Quantitative calculations of the many-body effects in real transition metals are beyond the scope of present theory, but have been qualitatively considered by Phillips (1965) and Spicer (1967). Many-body effects need not be invoked to explain the present data.

An analysis procedure for determining the optical density of states from the nondirect model has been given. Since the scattering correction is explicitly included, the analysis must be done in two steps: a zeroth and final approximation.

The analysis procedure is outlined below:

1. Zeroth approximation

- a. determine N_{io}^{opt} and N_f^{eff}
- b. calculate N_{fo}^{opt} from Eq. (2-46) using measured optical transition strength and N_{io}^{opt} .

2. Final approximation

- a. using N_{io}^{opt} and N_{fo}^{opt} with appropriate cut-off and extension, calculate effect of secondaries
- b. subtract secondary from EDC's
- c. determine N_i^{opt} from corrected EDC's
- d. repeat step 1.b. using N_i^{opt} .

III. EXPERIMENTAL PROCEDURES AND EQUIPMENT

A. Photoemission Measurements

The photoemission measurements of the present study were done on vapor deposited films produced and maintained under ultra-high vacuum conditions. The design of the electronic and vacuum equipment allowed studies of the EDC's and the relative quantum yield to be measured. The techniques and designs are explained in outline form unless they are unique to the present study. The reader is referred to the cited literature and manufacturer's manuals for more detailed explanations and characteristics.

1. Basic Experimental Apparatus and Procedures. A schematic diagram of the basic apparatus used for measuring the photoelectric yield and energy distributions is shown in Fig. 5. The photodiode consisted of two parts, the cylindrical collector and the disk-shaped photocathode constructed from type 304 stainless steel. The photocathode was highly polished with a small hole drilled through the center. The hole allowed a small fraction of the incident light to fall on a sodium salicylate (SS) coated glass window on the opposite wall of the chamber. The SS coated window was cooled to maintain the SS film at room temperature even when the system was baked. The photocathode was hinged so that it could be

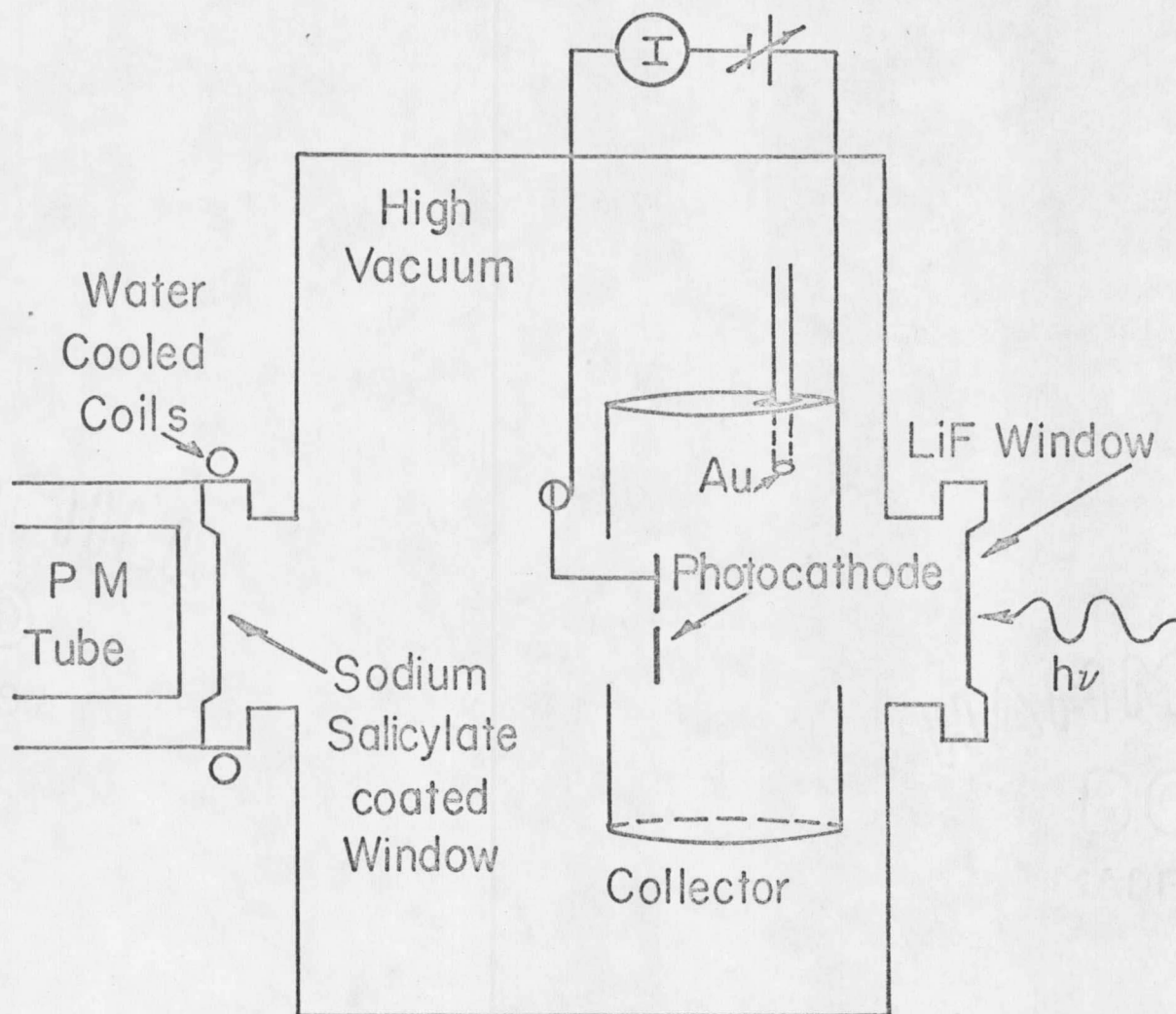


Fig. 5 . Schematic of Basic Apparatus Used in Photoemission Experiment.

withdrawn from the collector by means of a high vacuum linear motion feedthrough. In the withdrawn position a gold (Au) film was evaporated on the inside of the collector to assure a surface with an uniform photoelectric work function. Au was used to coat the inside of the collector because of its unique ability of maintaining its photoelectric properties even upon exposure to air (Krolikowski, 1967). The photocathode was withdrawn from the collector, and was coated with a film of the metal to be studied (cf. Fig. 6), before it was returned into the collector for the photoemission measurements.

The entire photodiode assembly was maintained in a high vacuum chamber ($\lesssim 5 \times 10^{-10}$ torr) to insure clean surfaces. Clean surfaces are needed to minimize scattering of the photoemitted electrons due to surface contamination. A high vacuum LiF window of design reported elsewhere (Kendig and Spicer, 1965), was used to transmit the radiation into the apparatus.

The radiation in the range 2.0 to 12.0 eV was supplied by a Hinteregger hydrogen discharge lamp dispersed by a one-meter normal incidence monochrometer (McPherson Model 225). Much higher radiation intensities were supplied in the 0.5 to 6.0 eV range by deuterium, mercury, and tungsten light sources dispersed by Bausch and Lomb 33-88 series monochrometers. For all energies used, the optical band was less than 0.1 eV.

2. Vacuum Equipment and Procedures. The only vacuum equipment and procedures described in detail will be those used in conjunction with the photoemission studies. The equipment and procedures used in the optical measurements were similar to that used for photoemission studies unless otherwise noted.

The stainless steel chamber housing the experimental apparatus was built from standard high vacuum fixtures and from a few custom modified fixtures, and is displayed in Fig. 6. All internal apparatus was constructed from low vapor pressure refractory materials such as non-magnetic 304 series stainless steel and OFHC-Cu. The selection of materials allowed the capability of baking the system to 200°C. Baking at elevated temperatures was necessary for the outgassing needed to achieve the desired high vacuum. The materials exposed to the high vacuum were carefully cleaned and handled according to standard high vacuum cleaning procedures (Rosebury, 1965).

The high vacuum system was initially evacuated by an oil free Vacorb (Varian) pump. The pressure was further reduced with the aid of an 8 l/sec VacIon (Varian) pump. High vacuum pressures were achieved and maintained by an 800 l/sec Orblon (Norton) pump. The pressure of the high vacuum system, as measured by Bayard-Alpert ionization gauge, was about 5×10^{-10}

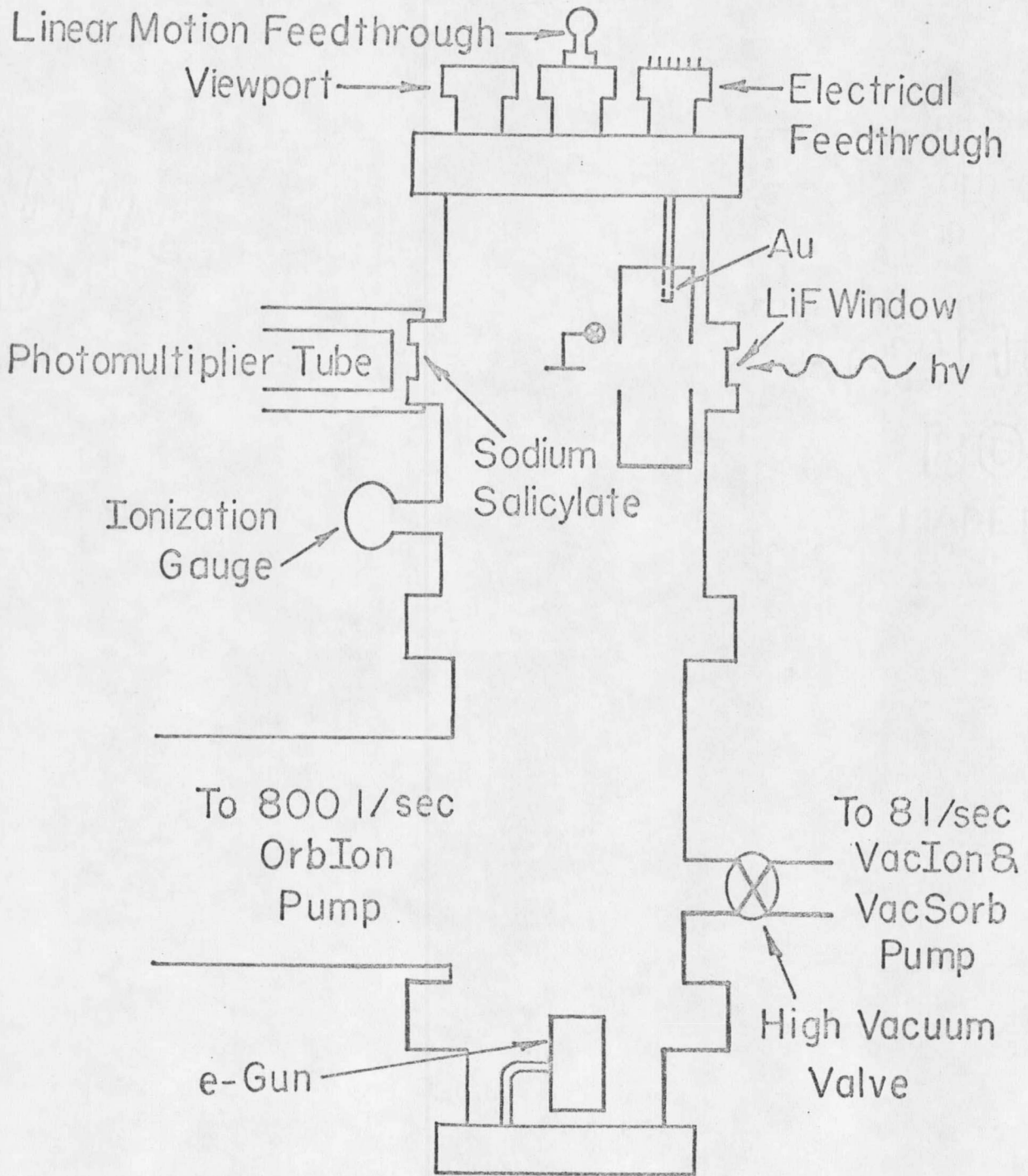


Fig. 6 . Schematic of Vacuum Chamber for Photoemission Studies.

torr after baking the entire system at $\approx 200^\circ\text{C}$ for 12 to 48 hours. Since the reflectometer had detectors which could not be baked above 75°C , only those portions remote from the detectors were baked at 200°C .

3. Sample Preparation. The photocathode was coated with a thick metal film ($\approx 1000 \text{ \AA}$) by vapor deposition under high vacuum. The metal sample was vaporized by a water cooled electron beam deposition gun (Varian) near the bottom of the chamber as seen in Fig. 6. When the electron gun and the metal sample had been carefully outgassed, evaporated films could be produced at 5×10^{-9} torr. The total evaporation time could not exceed several minutes because radiation from the molten refractory metals would heat and outgas the surroundings. These metal films were contiguous with the polished stainless steel photocathode and appeared visibly smooth. Subsequent x-ray powder patterns of samples scraped from the photocathode were characteristic of the polycrystalline pure metal.

4. Energy Distribution Curve Measurement. The kinetic energy distribution of the photoemitted electrons was measured by the retarding potential method. A potential difference that varied linearly with time was applied between the photocathode and the collector while the radiation incident on the photocathode was maintained at a constant flux level and wavelength,

Fig. 5. An operational amplifier differentiator was used to time differentiate the instantaneous signal from the electrometer monitoring the photocurrent (Kress and Lapeyre, 1968). The resultant signal is proportional to the number of electrons which have the same kinetic energy as the instantaneous potential difference across the photodiode, i.e. proportional to the kinetic energy distribution of the photoelectrons. The physical equipment and electronic details of this measurement have been published (Kress and Lapeyre, 1968).

A small contact potential was observed between the photocathode and collector (see Fig. 9). This small contact potential was known in both sign and magnitude since the work function of the collector (Au) is known and that of the photocathode was measured (Decker, 1954). The effect of the contact potential was eliminated from the measurements.

Experimental errors and uncertainties in the EDC measurement by the retarding potential method have been discussed in detail by other (cf. Eden, 1967 and Krolikowski, 1967). Their discussions are applicable to the present study if the errors and distortions due to the operational amplifier differentiator designed and built for the present study are included (Kress and Lapeyre, 1968). The overall effects of these errors and distortions produce an experimental uncertainty of

structure in the EDC of about ± 0.1 eV. The position of the Fermi energy is determined within similar experimental limits.

5. Quantum Yield. The absolute quantum yield, defined as the number of photoemitted electrons per absorbed photon, was measured by first determining the relative quantum yield per absorbed photon. The relative quantum yield can be determined if the photocurrent, normalized to the photon flux, and the reflectance are known as a function of photon energy. The total photocurrent is easily measured at a given flux level by maintaining a +10 volt potential between the collector and photocathode while monitoring the photocurrent with an electrometer. The photocurrent, I_p is given by

$$I_p = \frac{\ell(h\nu) Y(h\nu)}{1-R(h\nu)} \quad (3-1)$$

where $\ell(h\nu)$ is the incident photon flux, $Y(h\nu)$ is the absolute quantum yield, $1-R(h\nu)$ represents the fraction of the flux absorbed. The more difficult relative photon flux measurement was determined from the small fraction of the photon flux that passed through the photocathode and caused fluorescence of the SS coated window opposite the LiF entrance window as shown in Fig. 5. A photomultiplier tube (EMI 9514) outside the high vacuum chamber was used to monitor the fluorescence from the SS. Assuming the relative fluorescent quantum efficiency of SS is constant, the current from the

photomultiplier is

$$I_F = C \lambda(h\nu) \quad (3-2)$$

where C is the effective gain of the detection system. The signal from the photomultiplier tube was electronically divided into the photocurrent signal in a continuous manner by means of an operational amplifier voltage divider (Philbrick-Nexus). The output of the divider is proportional to the yield per incident photon,

$$V = C' \frac{Y(h\nu)}{1 - R(h\nu)} \quad (3-3)$$

where C' is a constant summarizing all the effective gain factors.

The divided signal described by Eq. (3-3) was recorded on the Y axis of an XY recorder as the photon energy was continuously changed with time. A signal proportional to the instantaneous photon energy, $h\nu$, was simultaneously recorded on the X axis (Kress, 1969). The recorded yield per incident photon (Eq. 3-3) was corrected by the measured reflectance to obtain the relative quantum yield per absorbed photon. The absolute yield was determined at 10.2 eV from the absolute light flux (NO cell, Melpar), the LiF window transmission, and the absolute photocurrent.

The above method of measuring the relative quantum yield

of a metal relative to the response of a SS film inside a high vacuum chamber appears to be unique to this work and will be considered further. There are two possible reported sources of error that result from using the relative fluorescent quantum efficiency of SS for the measurement of the light flux. Recent studies (Samson, 1967) indicate that a decrease in the efficiency of SS occurs in the wavelength region 1600 Å to 1000 Å (\approx 8 to 12 eV). This decrease is approximately 10 to 20 percent. In addition to the relative efficiency problem, some reports of time dependence of the relative efficiency of SS have appeared in the literature and were noted in this laboratory when SS was maintained in a vacuum produced by a diffusion pump. Contrary to these observations no aging was found in the present study (see below) and by others (Allison et al, 1964) when SS was maintained in an oil free, vacuum environment at room temperature.

The aging and flatness of the SS coating used in the Mo study was indirectly checked by comparing the yield of Au obtained by the above method with that obtained by means of a detector that was calibrated at several points with a vacuum thermopile (Krolikowski, 1967). Before comparing with the Krolikowski results, the relative yield per incident photon measured by the above technique was corrected with the published reflectance of Au (Canfield and Hass, 1965) and

arbitrarily normalized. The results are displayed in Fig. 7. The agreement over the measured range of photon energies is good.

The greatest experimental uncertainty of the relative quantum yield arises from the uncertainty in the relative fluorescent quantum efficiency of SS. Combining the estimate with the errors introduced by the electronic voltage divider, it is estimated that the absolute values of the yield reported may be in error by as much as 25% for energies remote from the one calibrated point (10.2 eV). Within a small (1 or 2 eV) energy range, however, the relative values of the yield have only several percent relative uncertainty.

B. Optical Measurements

The optical "constants" of a metal may be determined when the reflectance at near normal incidence is known over a wide range of photon energies and the reflectance at some angle other than normal incidence is known over a limited energy range (Appendix B). It is important that the surface of the metal remains clean during optical measurements since small amounts of contaminants have noticeable effects on the optical functions in the vacuum ultraviolet region (Beaglehole, 1965). The evaporated film, therefore, must be prepared and the reflectance measurement must be done in a high vacuum environment. A reflectometer which could meet

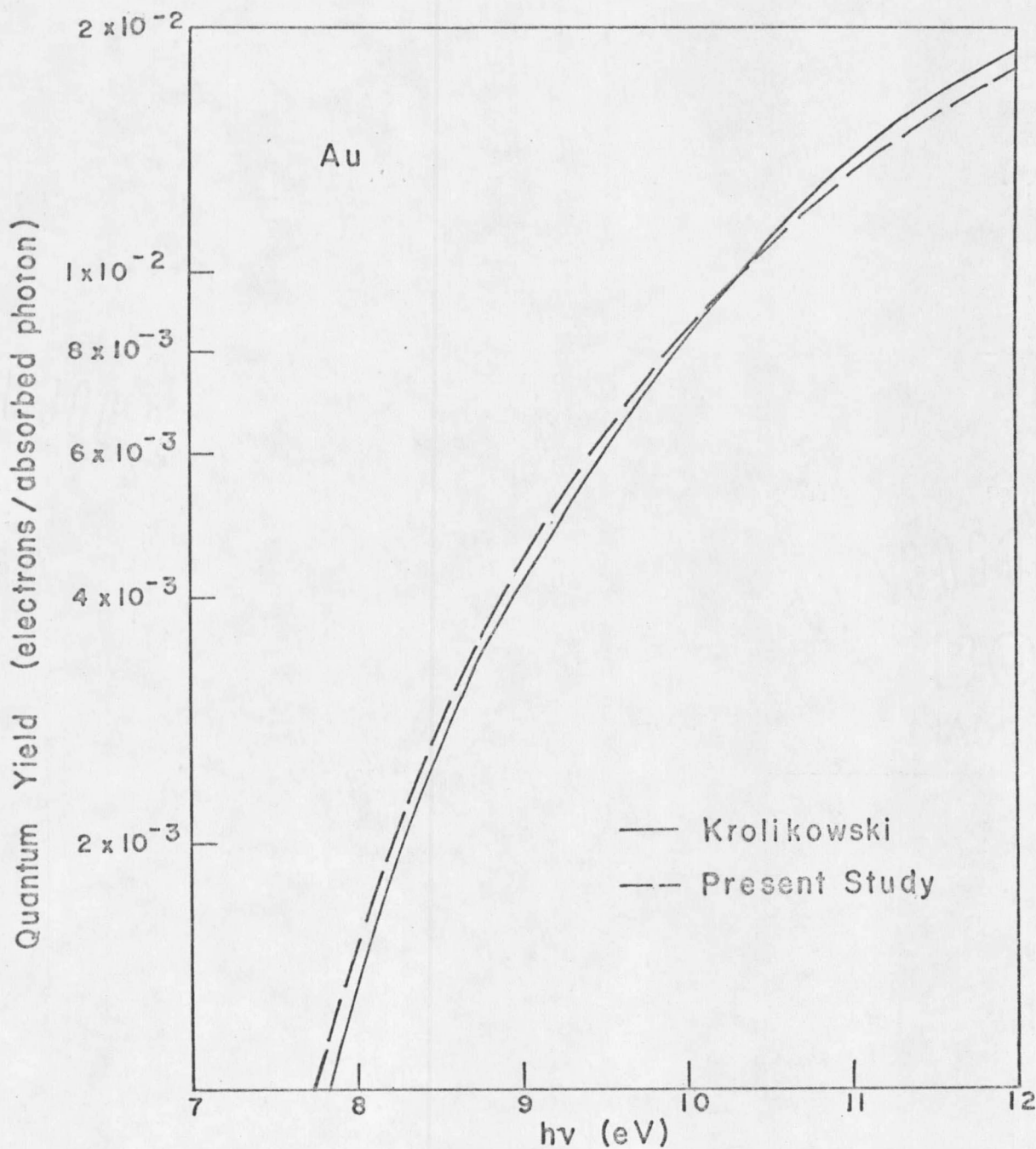


Fig. 7 . Quantum Yield of Gold Compared to That Taken by Krolikowski.

these requirements was constructed and is briefly described below.

1. Reflectometer. The reflectance measurements in this study were taken by means of a high vacuum reflectometer designed and built mainly by Lapeyre, Holverson, and Stensland (1969). A schematic diagram of the reflectometer and vacuum system used in the present study is presented in Fig. 8. The smaller 250 l/sec VacIon (Varian) pump produced base pressures and evaporation pressures very similar to the 800 l/sec OrbIon (Norton) pump used in the photoemission studies.

The reflectometer was designed to allow the reflectance at arbitrary angles between 12° and 70° to be observed as described below. After coating the substrate (a clean microscope slide) by means of vapor deposition of the appropriate metal, the substrate was rotated to a horizontal position as shown by the dashed line in Fig. 8. The detector was then moved into the light and rotated until the maximum obtainable signal was found (dashed circle). The substrate was moved to the desired angular position and the detector was rotated until its signal was maximized again. The position of the detector indicated the angle of reflectance and the ratio of the above two signals was recorded as the reflectance.

Two detectors were used to span the complete energy

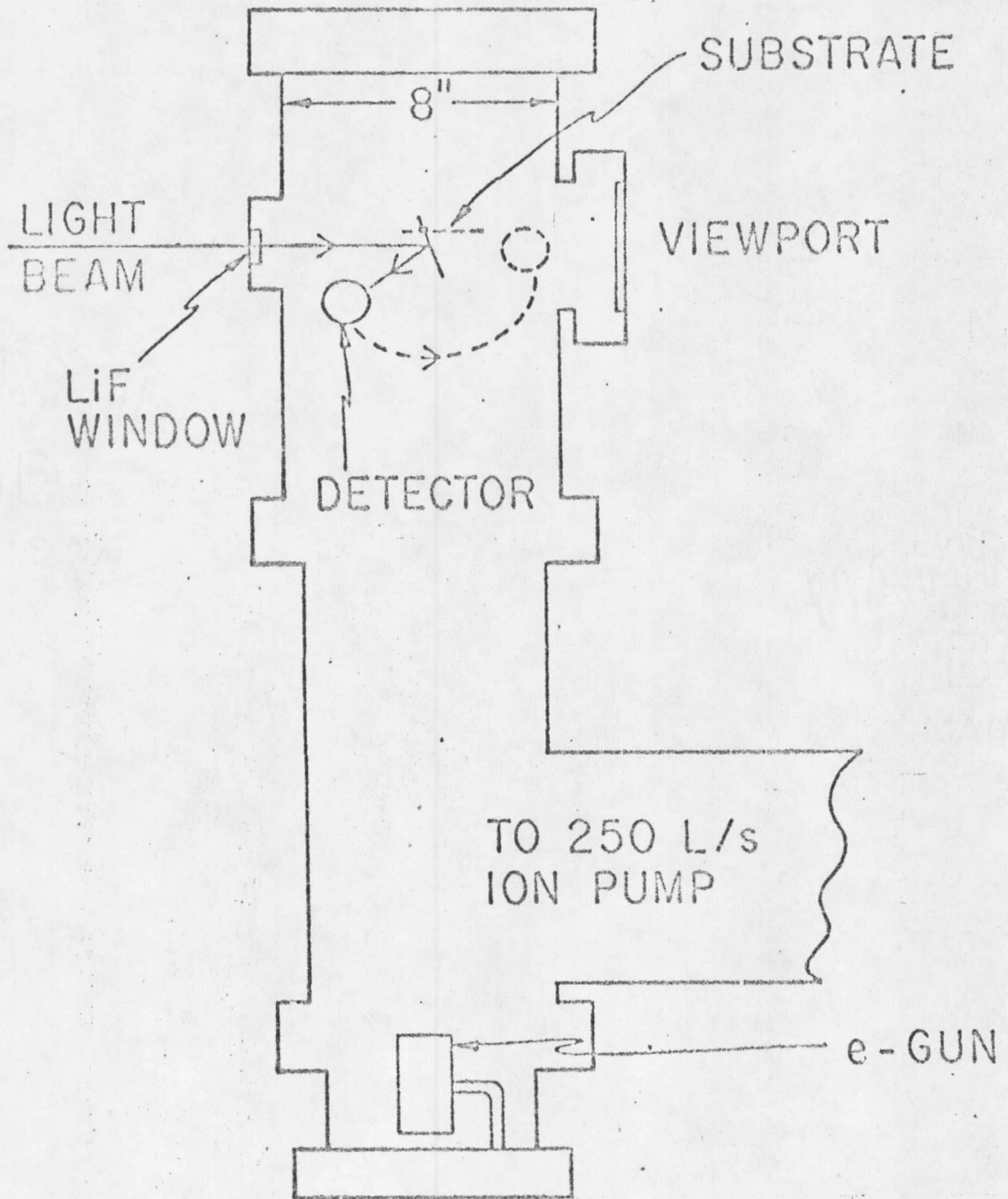


Fig. 8 . Schematic of Reflectometer Used for Reflectance Measurements.

range of interest. From 2.0 eV and 12.0 eV a 1P28A photo-multiplier (PM) with a thin SS coating was mounted inside the reflectometer. In the ultraviolet region, the fluorescence of the SS film provided the detectable signal for the PM. Below 6.0 eV the envelope of the PM and the thin SS film was semi-transparent and allowed the incident radiation to fall directly on the photocathode of the PM.

Since the threshold energy for the PM is approximately 2.0 eV, another detector was needed to extend the optical measurements below 2.0 eV. An Eastman Kodak lead sulfide (PbS) (1 x 5 mm) detector was chosen to extend the range of the reflectance. The PbS detector was sensitive from 0.5 eV to 3.0 eV. PbS has a high vapor pressure and was kept from evaporating by means of a glass coverplate sealed by Varian's Torr Seal. The Torr Seal raised the base pressure in the reflectometer to $\approx 2 \times 10^{-9}$ torr. In spite of the degraded base pressure, the data obtained in the near infrared region reproduced the high vacuum data where they overlapped indicating a lack of contamination.

Errors and uncertainties in the reflectance measurement at normal incidence were checked by measuring the reflectance of Cu between 2.0 eV and 12.0 eV. These observations reproduced the published Cu data within $\pm 2.5\%$. The absolute value of the reported reflectance is thus not expected to be

greater than $\pm 2.5\%$. The relative values of the reflectance are considerably better. There is no simple relation between the uncertainties in the reflectance and the optical constants (Beaglehole, 1965).

C. Data Reproducibility

Reproducibility of the structure and magnitude of all the photoemission and optical data was the minimum criterion used to determine a "good" set of data. The metal films were evaporated with the experimental chamber coupled to the light source and all the electronic measuring and recording apparatus were operating for both the photoemission and optical studies. Within one minute of completing a film, the initial measurements were taken. The first measurement was retaken periodically as a check on any aging effects. In general, there were no observable aging effects over a four to eight hour period when the base pressure was in $\approx 5 \times 10^{-10}$ torr range and deposition occurred in the 10^{-9} torr range. If the films were maintained for longer periods, small changes would appear indicating contamination of the metal surface by the residual gasses in the vacuum chamber.

The observed aging effects were small and did not change the major features of the EDC or the quantum yield. This assertion is illustrated by the EDC's in Fig. 9, plotted directly from the experimental charts. Mo film IV was about

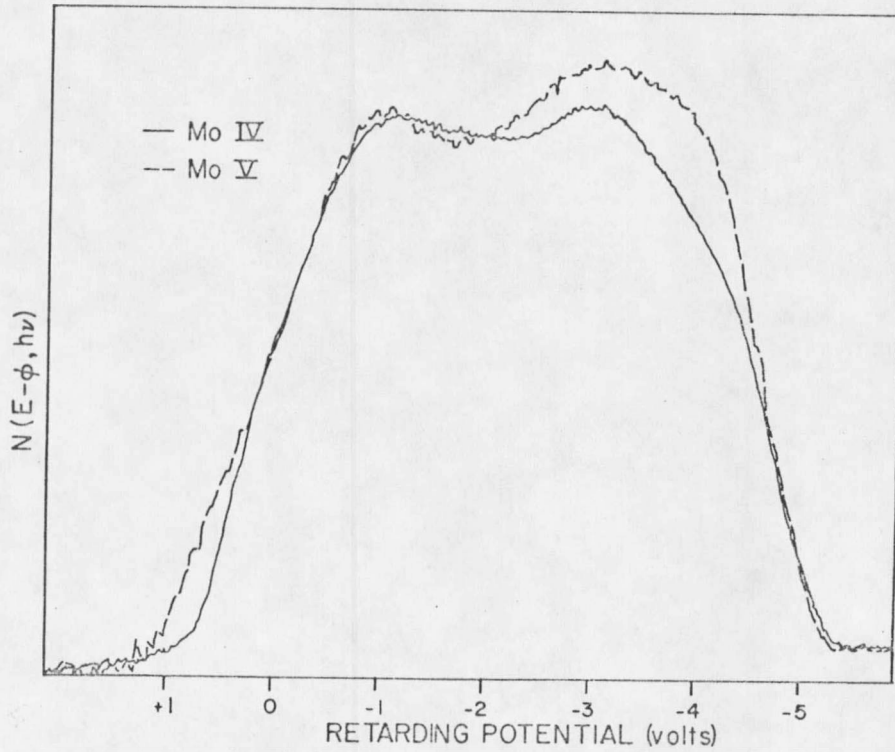


Fig. 9 . Direct Tracing of Experimental Energy Distribution Curves for $h\nu = 10.2$ eV from Experimental Chart.

24 hours old when the illustrated EDC was taken. Film V was evaporated over Film IV and the EDC immediately retaken with all the same experimental parameters except for an 8% increase in lamp current needed to stabilize the lamp. It is apparent that the fraction of high kinetic energy electrons is decreased in the EDC of film IV as compared to that of Film V. Since the width of the EDC from Film V is 0.3 volt less than that of Film IV, the photoelectric work function is less. If the area of the EDC from Film V is decreased by 8% to compensate for the change in the lamp intensity, the difference in the areas of the two EDC's is a direct measure of the difference in the quantum yield. The difference is very small. The above results are typical of the aging observed.

The reproducibility of the measured work function was not good in the initial measurements. It had been assumed that the yield and threshold function measurements were less sensitive to surface contamination than the EDC's measurement. Hence EDC's were taken, then the threshold and yield data. When the order of data taking was changed and the threshold data completed first, the threshold measurement became very reproducible.

Reproducibility of the reflectance data was relatively insensitive to evaporation pressures and aging effects. Evaporations in the 10^{-8} torr range would agree well with

those done in the 10^{-9} torr range. The overall magnitude of the entire reflectance curve obtained from individual films was shifted by 1 to 2% from the average magnitude. These shifts did not correlate with the evaporation or base pressures. Although the magnitude of the various samples had some film dependence, the structure observed in the reflectance from different films reproduced on all the observations. It was concluded that these shifts in magnitude were due to the nature of the metal film itself.

IV. MOLYBDENUM EXPERIMENTAL RESULTS

A. Optical Measurements

In the present chapter, the results of optical and photoemission measurements of the metal molybdenum (Mo) are presented. The experimental procedure used to obtain the following measurement is given in Chapter III. The definition of the functions with their theoretical development is given in Chapter II. Discussions relevant to the analysis procedures are given here. Interpretation of the results is mainly reserved for Chapter VI.

1. Reflectance. It is shown in the theory section and in Appendix A that the optical constants may be derived from the reflectance at near normal incidence and a segment of the reflectance at another angle. Such measurements were taken between 0.5 eV and 11.9 eV on four vapor deposited films of Mo as described in Chapter III, and are summarized in Fig. 10 (solid line). The best evaporation pressure was $\approx 5 \times 10^{-9}$ torr with a base pressure of $< 5 \times 10^{-10}$ torr. The films were produced from samples obtained from two sources: Jarellash Company (99.99% pure), and Materials Research Corporation (99.995% pure, in particular less than 15 parts per million carbon). The reflectance from a mechanically polished bulk sample purchased from Sylvania Corporation (99.5%) was also obtained at near normal incidence between 2.0 eV and 14.0 eV.

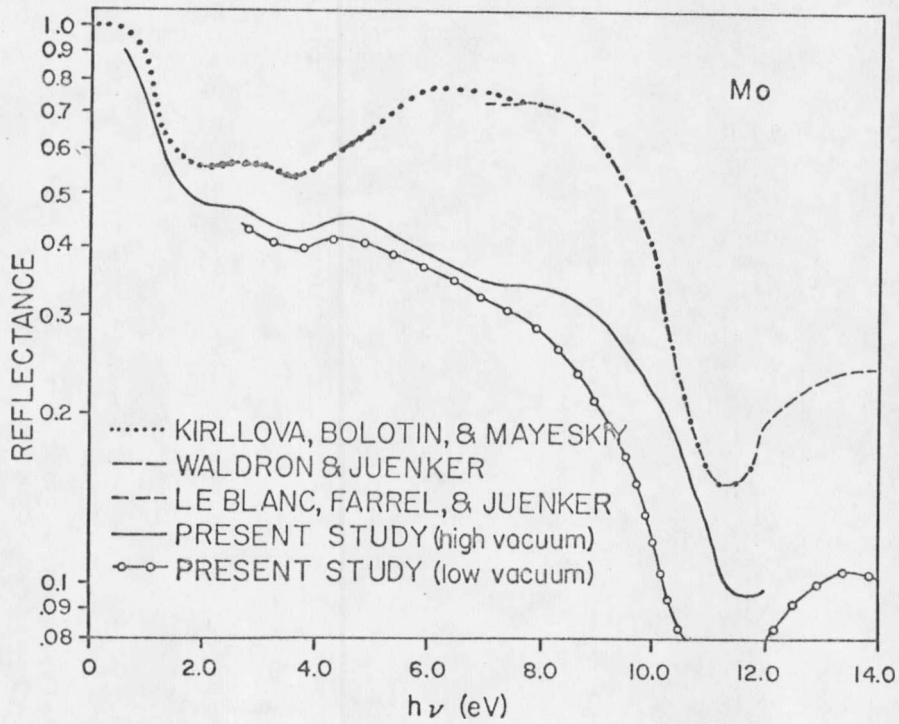


Fig. 10. Summary of Reflectance Measurements for Molybdenum.

The reflectance of Mo has been measured by others. Kirillova et al. (1967) used mechanically polished bulk samples exposed to the atmosphere to find the reflectance between 0.05 eV and 12.0 eV. Waldron et al. (1964) measured a heat cleaned bulk sample in a high vacuum glass tube between 2.0 eV and 5.0 eV. LeBlanc et al. (1964) used a heat cleaned bulk sample in a high vacuum stainless steel chamber and photoemission technique to obtain the reflectance between 6.0 eV and 23.0 eV. These other studies agree well with each other but differ from the present study as seen in Fig. 10. The disagreement requires some discussion.

The data of Waldron et al. and LeBlanc et al. were taken under high vacuum conditions ($\approx 10^{-9}$ to 10^{-10} torr). Their sample consisted of a bulk sheet of Mo which was cleaned before placing it in the high vacuum. Under high vacuum conditions, the Mo was flashed to a very high temperature ($\approx 2200^\circ\text{K}$) immediately before taking reflectance measurements. The assumption was made that this severe heating would produce a clean surface of Mo since most materials evaporate more rapidly than Mo at these elevated temperatures. This is not true of carbon, which has a vapor pressure versus temperature dependence almost identical with Mo (Rosebury, 1965). Some of the more recent literature on Auger electron emission from Mo (Vance, 1967) indicates that carbon contamination of the

surface of Mo is increased by diffusion of carbon from the bulk material when a bulk sample is heated to high temperatures in a high vacuum environment. The above observations indicate the optical data obtained from heat treated bulk samples of Mo should be treated with caution.

To check the data reported by Kirillova et al, the reflectance of a mechanically polished (Al_2O_3 polishing grit) bulk sample was also measured in the present study in a low vacuum reflectometer designed and built by others (Chor, 1967). The results of the low vacuum reflectance measurement are seen in Fig. 10. This measurement did not reproduce the data of Kirillova et al. or that of Waldron and LeBlanc. It did reproduce all the structure of the high vacuum data taken in the present study with a small attenuation in the general magnitude of the reflectance. Since unusual carbon contamination of sample prepared by mechanical polishing is not expected, it is difficult to understand the differences between these observations and those of Kirillova et al.

The agreement between reflectance measured from the air-exposed mechanically polished bulk sample and the evaporated films formed under high vacuum conditions, was taken as confirmation that the high vacuum results of the present work are the best measurements of the reflectance of Mo for $0.5 \text{ eV} < h\nu < 12.0 \text{ eV}$ at this time. This conclusion is

supported by the observed similar magnitudes of the reflectance of the high vacuum Mo data of the current study and that of W (LeBlanc et al, 1964). The optical properties are expected to be similar since the electronic structure of Mo and W are similar.

The optical constants of Mo have been extended to 23.0 eV by use of LeBlanc's reflectance data. His reflectance curve was multiplied by the constant needed to join his curve smoothly to the reflectance measured in this work at about 12 eV. The results are given in Fig. 11. This procedure is justified by the empirical observation that the addition of LeBlanc's data beyond 12.0 eV does not significantly change the calculated optical constants of Mo below 12.0 eV compared with the results obtained by cutting the measured reflectance off at 12.0 eV. No interpretation made in this study will depend on the optical functions beyond 12.0 eV.

The optical constants of Mo were calculated by Kramers-Kronig's analysis of the reflectance. The analysis can be completed only if a high photon energy extrapolation of the reflectance is assumed. The best fit, as explained in Appendix A, for the measured reflectance at 50° angle of incidence was obtained with an extrapolation of the form $R \propto (1/E)^{3.02}$ for $E > 23.0$ eV. Given this extrapolation $n(h\nu)$ and $k(h\nu)$ were found and all the other optical constants calculated from $n(h\nu)$ and $k(h\nu)$.

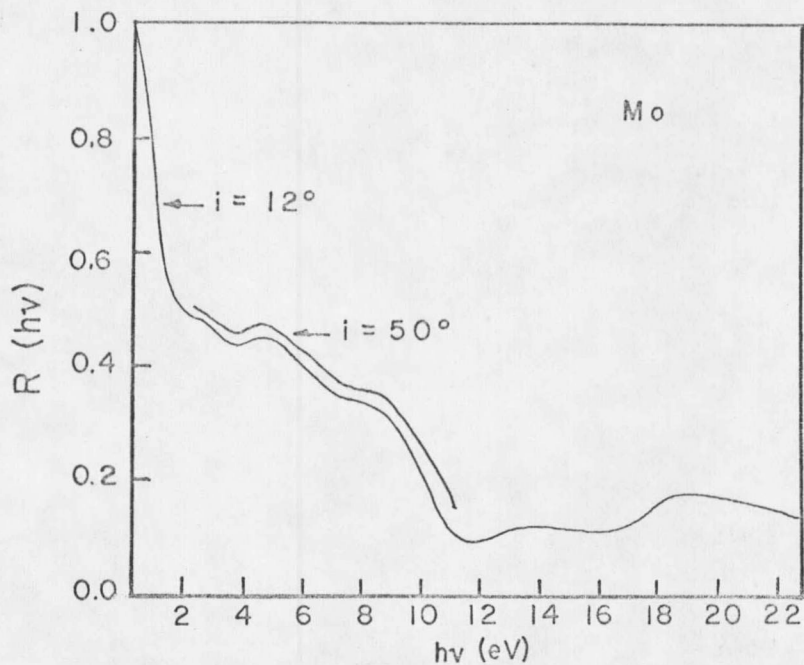


Fig. 11. Reflectance of Molybdenum Where i Is the Angle of Incidence.

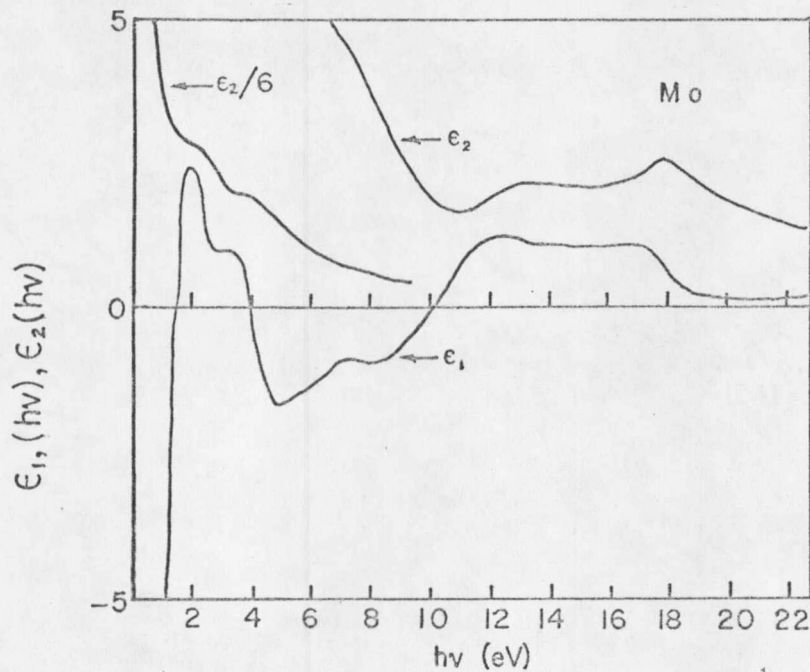


Fig. 12. Dielectric Function of Molybdenum.

The high energy extrapolation introduces some error into the optical constants since the exact high energy reflectance is not determined. The error introduced by the high energy extrapolation produces some uncertainty in both the magnitude and energy position of structure in the optical constants. The energy position of structure in the optical constants was found to be insensitive to large changes of the exponent in the high energy extrapolation. The magnitude of the optical constants was more sensitive to the value of the exponent. The magnitude of the present calculation for $n(h\nu)$ and $k(h\nu)$ are compared with values measured by techniques that did not depend on a high energy extrapolation in Table I. Considering

TABLE I

Energy	Optical constant		Study
	n	k	
2.15 eV	3.1	2.6	(Present study)
	3.2	3.4	(Juenker et al, 1968)
	3.6	3.3	(Summer, 1934)
	4.4	3.6	(Waldron and Juenker, 1964)
1.00 eV	3.0	4.1	(Present study)
	3.0	4.8	(Kirillova et al, 1967)

the magnitude differences observed in the reflectance of Mo compared with the reflectance observed in the studies summarized in Table I (cf. Fig. 10), the agreement is reasonable.

2. Dielectric Constant. The real part, $\epsilon_1(h\nu)$, and the imaginary part, $\epsilon_2(h\nu)$, of the complex dielectric constant or response function is presented in Fig. 12. If the electrons in the metal had free electron character only, ϵ_2 would monotonically fall to zero while ϵ_1 would monotonically rise to one with increasing energy (cf. Eq. (2-10)). Deviations from the rapid fall in ϵ_2 are centered at 1.8 eV and 3.8 eV. The marked deviation of ϵ_1 from the free electron-like, monotonic rise towards unity begins early (1 to 2 eV) and ceases near 5 to 6 eV. The behavior of ϵ_1 indicates numerous transitions below 6 eV.

The location of the beginning of the interband transitions in Mo is not possible from the present studies of $\epsilon(h\nu)$ since these measurements extend only to 0.5 eV. Lenham (1965) however, studied the infrared behavior of the optical function $2nk/\lambda$ and found the interband threshold to be 0.44 eV. Furthermore, Lenham found that optical constants of Mo were not free electron-like within the limits of his measurements (≥ 0.1 eV). Kirillova et al (1967) also studied the infrared optical functions. They found that the onset of the interband transitions began at 0.17 eV. In either case, the optical

functions of Mo, as the optical functions of most of the other transition metals (Lenham, 1965), do not have free electron character even in the near infrared region.

The lack of free electron-like behavior for the optical functions of Mo in the range 0.5 eV to 2.0 eV was verified in the present study. Attempts were made to separate the free and bound electron contributions to the dielectric function as has been done with the noble metals Ag and Cu (Ehrenreich and Philipp, 1962). That is, the free electron expression for ϵ_f , Eq. (2-11), was fitted to the experimentally determined ϵ in the range 0.5 to 2.0 eV by considering τ , the relaxation time, as a parameter. It was found, however, that τ could not be considered a constant, i.e. τ had energy dependence.

3. Loss Functions. The energy of collective volume and surface excitation is determined from the peaks of the volume and surface loss functions respectively, since the optical constants satisfy the conditions presented in detail in Chapter II. A peak in the volume loss function, $\text{Im } 1/\epsilon$ (where Im denotes "imaginary part of"), occurs at 10.8 eV while that of the surface loss function, $\text{Im } 1/(\epsilon+1)$, occurs at 9.9 eV as seen in Fig. 13. The energy of volume plasmon resonance is in rough agreement with that found by LeBlanc at 10.0 eV. This energy is also in reasonable agreement with characteristic

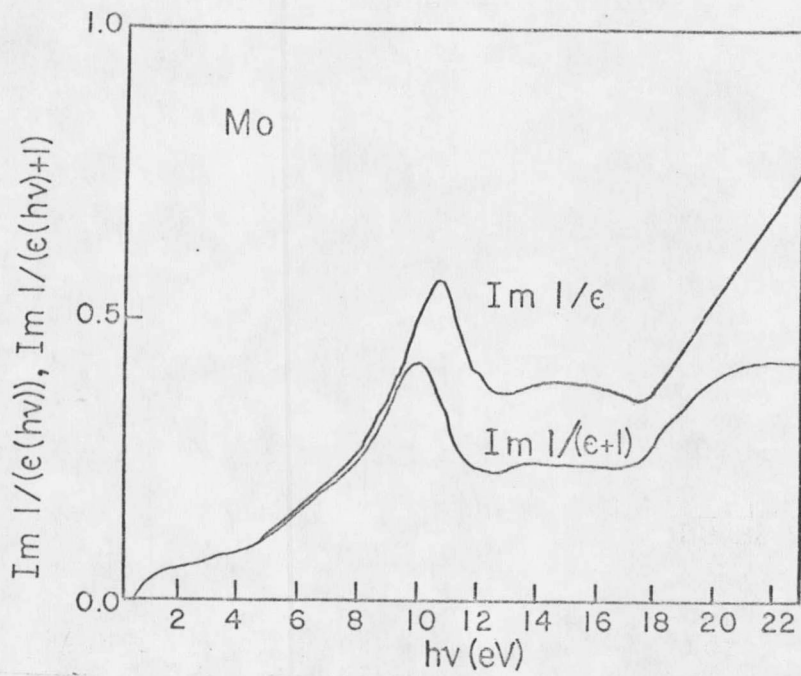


Fig. 13. Loss Functions for Molybdenum.

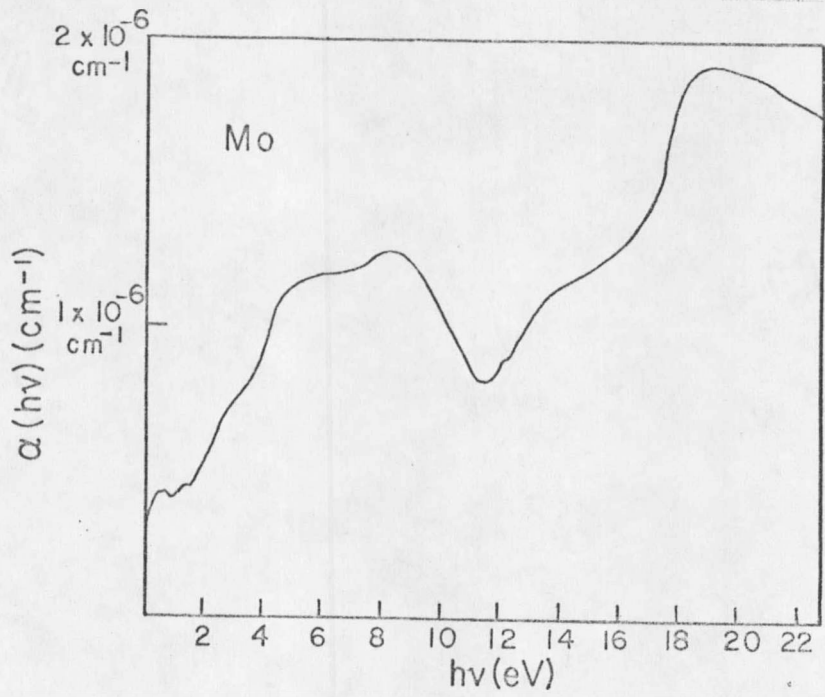


Fig. 14. Absorption Coefficient α for Molybdenum.

energy loss measurements of fast electrons reflected from Mo. Haworth (1935,1936) found peaks in the characteristic energy loss spectrum of Mo at 10.6 eV and 22.0 eV. Kleiner (1954), on the other hand, found them at 12.0 eV and 24.5 eV. The lower value of Haworth is in good agreement with this study and that of Kleiner in rough agreement. Neither Haworth nor Kleiner resolved two peaks, one due to the volume and the other due to the surface excitation. In general, collective oscillations are determined with better resolution from optical experiments than from characteristic energy loss studied for low and medium energy ($\lesssim 25$ eV) excitation (Arakawa et al, 1965).

Assuming six free electrons per atom for Mo, the free electron model gives $h\nu_p \approx 23$ eV. LeBlanc's optical investigation beyond the energy range of this study is consistent with a classical plasma resonance in this energy region.

4. Alpha, $(h\nu)n(h\nu)$, $(h\nu)^2 \epsilon_2(h\nu)$. The optical functions $\alpha(h\nu)$ and $(h\nu)n(h\nu)$ and $(h\nu)^2 \epsilon_2(h\nu)$ are displayed in Fig. 14 and Fig. 15 respectively. The absorption coefficient, $\alpha(h\nu)$, has a relative minimum for $h\nu = 11.3$ eV. Consequently, the mean excitation depth for electrons is a maximum at this energy. The optical functions $(h\nu)n(h\nu)$ and $(h\nu)^2 \epsilon_2(h\nu)$ have large differences in magnitude, but only small differences in shape. These functions will be used in the analysis of the photoemission data.

